



Manganese oxide nano-platforms in cancer therapy: Recent advances on the development of synergistic strategies targeting the tumor microenvironment

Javier Bonet-Aleta^{a,b,c}, Javier Calzada-Funes^{a,b,c}, Jose L. Hueso^{a,b,c,*}

^a Instituto de Nanociencia y Materiales de Aragon (INMA), CSIC-Universidad de Zaragoza, Zaragoza 50009, Spain

^b Department of Chemical and Environmental Engineering, University of Zaragoza, C/Poeta Mariano Esquillor, s/n; Campus Rio Ebro, Edificio I+D, Zaragoza 50018, Spain

^c Networking Research Center on Bioengineering, Biomaterials and Nanomedicine (CIBER-BNN), Instituto de Salud Carlos III, Madrid 28029, Spain

ARTICLE INFO

Keywords:

Manganese oxide nanoparticles
Tumor microenvironment
Oxygen
Glutathione
Starvation therapy

ABSTRACT

The use of inorganic nanomaterials to tackle and exploit the intrinsic chemical nature of the tumor microenvironment (TME) has emerged as a promising strategy in cancer therapy. Manganese oxide nanoparticles (Mn_xO_y) offer unique advantages in terms of redox properties and specificity towards the TME scenario: low O_2 concentrations, mildly acidic pH and high oxidative stress; environmental conditions that often lead to a reduction in the efficacy of cancer treatments. Mn_xO_y -based nano-platforms have recently demonstrated exciting properties as inorganic nanocatalysts to operate under TME constraints. Alternatively, Mn-nanocatalysts have also displayed synergistic anticancer response in combination with other active co-adjuvant elements (drugs, enzymes or nanomaterials). The aim of this review is to provide new insights on the main functionalities of Mn-based nanomaterials applied to cancer therapy. We analyze its capacity as oxygen supplier in hypoxic scenarios, its role to induce the selective depletion of glutathione (GSH) to maximize cell stress or its capacity to promote starvation therapy via glucose oxidation. We aim at providing an insightful view of the operating mechanisms behind each of these critical processes and highlight the versatility and catalytic richness of Mn-based nanoparticles in this developing field. We also provide a general and comprehensive analysis of the Mn fate when trafficking through the intracellular levels.

1. Introduction

Cancer constitutes one of the main causes of death despite the wide range of existing therapies. Forecasts for 2030 are not optimistic since ca. 21.7 M of new cases and 13 M of deaths are expected [1]. Current treatments include surgery, chemotherapy (CT) and radiotherapy (RT). However, they still face serious challenges. In the case of surgery, apart from the high risk related to infections, recent studies indicate that surgery may trigger new metastatic spotlights [2]. Patients treated with CT suffer from severe adverse effects due to the lack of specificity of CT drugs as they also affect healthy cells [3]. Finally, applying RT can damage tissues surrounding the tumor, and the lack of a continuous oxygen supply limits the treatment efficacy [4]. The optimization of current therapies (e.g. CT or RT) and the development and innovation of alternative treatments (e.g. photodynamic therapy (PDT), starvation

therapy (ST) or chemodynamic therapy (CDT)) focused on altering the intrinsic tumor microenvironment (TME) conditions [5,6] (see Fig. 1a) continue to be a great focus of intense research in the biomedical and oncologic fields.

Tumor growth entail a dramatic increased blood vessel formation (angiogenesis) [7] in order to maintain the accelerated metabolism of cancer cells, providing them with nutrients (especially glucose [8]) and oxygen (O_2) [9]. However, rapid growth provokes an irregular alignment of tumor associated endothelial cells within the tumor, with two main consequences: (i) large spaces between cells are created, with enough margin for 20–200 nm-sized nanoparticles to penetrate into the interstitial space, known as Enhanced Permeability and Retention (EPR) effect [10] and (ii) limited O_2 levels supply inside tumor cells (hypoxia conditions) [9]. In addition, the TME typically implies: (i) elevated oxidative stress levels [11]; (ii) higher H_2O_2 concentrations [12–15]

* Corresponding author at: Instituto de Nanociencia y Materiales de Aragon (INMA), CSIC-Universidad de Zaragoza, Zaragoza 50009, Spain.

E-mail address: jlhueso@unizar.es (J.L. Hueso).

than in healthy cells; (iii) lower pH values [16], (iv) larger glucose consumption rates [8]; (v) lower O_2 concentrations; (vi) over-expression of glutathione (GSH) [17–19], which reacts with the hydrogen peroxide (H_2O_2) generated as by-product in multiple cell processes (mitochondrial respiration or peroxisome metabolism, among others) [20,21] to avoid further cell damage (Fig. 1a).

All these features tend to negatively interfere on the effectiveness of cancer treatments based on irradiation [22] such as RT or PDT [23,24]. For instance, these therapies use O_2 as a reagent to produce ROS inside tumor cells, inducing their apoptosis. The limited supply of O_2 and the large GSH concentration burdens the optimal performance of these treatments. Thus, both *in situ* tumor O_2 generation (as a strategy to increase ROS production) and GSH depletion (as a way to prevent ROS depletion in cell intrinsic detoxification processes) are considered as appealing strategies to improve the efficiency of these cancer therapies [19,25]. On the other hand, the uncontrolled growth of tumor cells demands an accelerated metabolism that ends up in high glucose uptakes necessary to satisfy both energy and anabolic requirements. This phenomenon is known as Warburg Effect [8] and it is currently subjected to intense research that will be partially overviewed in forthcoming sections of this review. Emerging starvation therapies focus their efforts in selectively private cancer cells from glucose supplies so that cell growth can be inhibited [26]. Some approaches take advantage of the high activity and selectivity of natural enzymes to foster desired chemical reactions leading to deplete critical cell nutrients with the aid of glucose oxidase (GOx) [27] or lactate oxidase [28], among others.

New trends in Nanomedicine are aiming at designing novel nanostructured catalysts with enzyme-like behavior and are so-called

nanozymes [29–31] that may overcome typical enzyme drawbacks (high costs in production, purification and recovery processes [32]). Mn_xO_y -based nanoplateforms have emerged as promising candidates in cancer treatment due to their low cost, high and versatile catalytic activity and wide synthetic possibilities [24,25,33–37]. Mn exhibit a wide variety of oxidation states (from Mn^{2+} to Mn^{7+}) and offers a rich redox catalytic chemistry [38–40] that can be especially suitable for the previously described demanding environments of tumor cells. For instance, the high oxidation potential of Mn^{4+} promotes the reaction with GSH, which is overly present in TMEs [17] (Fig. 1a). As it will be discussed later, Mn chemistry can be suitable to catalyze GSH depletion and maximize the action of other antitumoral agents. MnO_2 nanosheets (NSs) are able to catalyze glucose oxidation into gluconic acid and H_2O_2 [41–43] and have been exploited as starving-catalyst for cancer therapy. Several Mn_xO_y -based nanoplateforms ended up as Mn^{2+} ions after its reaction with GSH. Freestanding Mn^{2+} species are able to catalyze the oxidation of organic molecules aided with H_2O_2 at pH values closer to physiological (7.4) [44] in comparison with Fe and Cu-oxides, which possess their maximum activity at more acidic pH (2–6) [45]. Alternatively, freestanding Mn^{2+} species may play a positive role in immunotherapy [46–48].

Focusing on cancer therapy, Mn_xO_y is responsive to TME chemical conditions given the inherently high H_2O_2 /GSH/ H^+ concentrations in TME [50], thereby enabling a strong potential cytotoxic action towards cancer cells by itself (Fig. 1a). According to the Pourbaix diagram displayed in Fig. 1b, MnO_2 (or even other lower valence Mn based oxides) possesses higher standard redox potentials (E_{SHE}) in the pH range typically observed in TMEs (i.e. 5.5–7.4) that favors thermodynamically

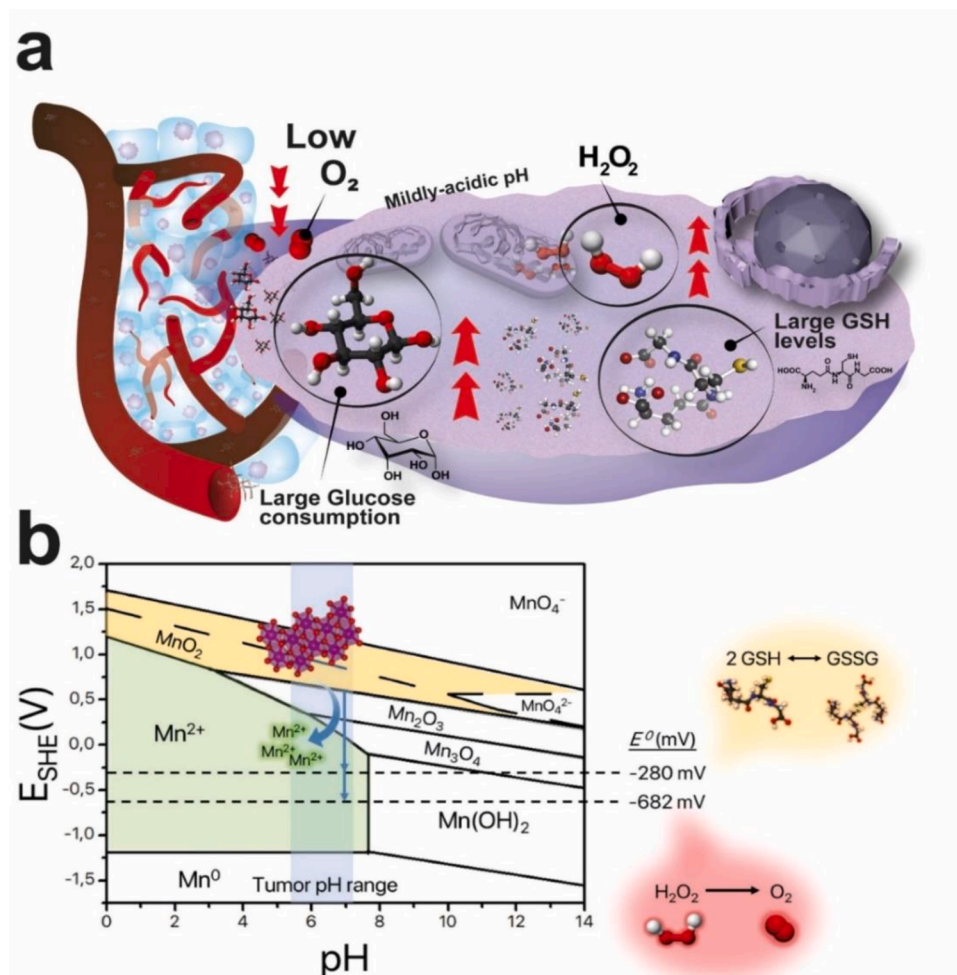


Fig. 1. Relevant chemical and working conditions for Mn-based nanomaterials in a Tumor Microenvironment. (a) Representative features defining the chemistry in TMEs. The chemical environment in tumors is different from that in healthy cells, exhibiting higher H_2O_2 and GSH concentrations, lower pH and hypoxic conditions with limited O_2 supply; (b) Pourbaix diagram [49] corresponding to different Mn-oxide species. MnO_2 is the most reported Mn-based nanomaterials in cancer therapy. The highlighted regions correspond to the pH ranges that are relevant in tumor environments. MnO_2 possess high standard redox potentials (E_{SHE}) in the physiological tumor conditions allows the reaction with GSH ($E^0 = -0.280$ V) or H_2O_2 ($E^0 = -0.682$ V) since the specific redox potentials are favored. Moreover, the thermodynamically favored product of those reactions is Mn^{2+} , avoiding bio-accumulation of Mn-based nanostructures.

their redox reaction with those abundant species in tumors (GSH or H_2O_2). Furthermore, because of their chemical reactivity under TME conditions, Mn_xO_y nanostructures degrade in tumor cells to thermodynamically more favorable Mn^{2+} ionic species thereby enabling an easier excretion from the organism. Shi's group demonstrated that nanoplat- forms with a slow biodegradation rate such as hollow mesoporous silica nanoparticles (HMSN) containing MnO_2 can also be degraded faster in tumor cells due to the defects generated as consequence of Mn_xO_y evolution towards their ionic form that enables rapid clearance and biodegradation [51]. Regarding to biocompatibility and biosafety, several studies endorse Mn_xO_y (at certain dosage) with low or negligible cytotoxicity (i.e. Hematoxylin and eosin stain (H&E), hematology or biochemical studies) on normal tissues [52–55].

Biomedical applications require both biocompatibility and colloidal stability in physiological media [56]. Generally, bare Mn_xO_y nanostructures lack of stability and tend to aggregate, reducing significantly their activity and in consequence their therapeutic effect. The synthetic versatility provided by Mn enables a flexible and versatile surface chemistry for potential interaction with a wide range of organic molecules to enhance both requirements (summarized in Fig. 2, Tables 1 and 2). Polyethylene glycol (PEG) either deposited directly [53,57–61] or through a Layer-by-layer process [52,62–65], is the most employed option, however, hyaluronic acid (HA) [66,67] or bovine serum albumin (BSA) [68–70] have also been reported in literature. Even new trends in NP delivery as cell mimicking are being applied to Mn_xO_y , which consists in cloaking the surface of the NPs with cell membrane fragments to enhance tumor delivery and biocompatibility [46,71–73]. Nevertheless, since a high percentage of Mn-based oxides for cancer therapy is combined with other metal nanoparticles, it is difficult to establish an ideal

surface modification.

The present work aims at providing an insightful view of the recent advances and trends on the chemical properties of Mn_xO_y nanoplat- forms playing a relevant role in specific processes of interest in TME, which may pave the way towards the development of novel cancer treatments. The focus on this single platform is far from narrow since these materials exhibit multiple synthesis possibilities, low production costs, high chemical versatility and strong chemical response. We intend to high- light the great potential hold by a variety of Mn-based materials and their synergetic combination with other active agents (i.e. drugs, photosensitizers (PS), other enzymatic platforms) (see Fig. 2). This review also intends to complement and enrich other recent review studies referred to Mn-systems [24,33] by establishing a detailed discussion on the role of Mn as a reactant or as catalyst, the identification of radical formation mechanisms, novel anticancer approaches or a clear assess- ment of the TME scenarios. The different sections of the review have been structured according to current state-of-the-art studies that have explored the specific response of Mn_xO_y as inorganic catalysts in tumor environments via: (i) *in situ* locally induced supply of O_2 levels in hypoxic tumors; (ii) decreasing intracellular GSH levels to disrupt redox equilibrium in tumor cells or (iii) altering the metabolism of cancer cells by targeting the glucose income and inducing a starvation therapy.

2. Mn_xO_y nanomaterials for local oxygen supply in tumor microenvironments

Tumor acute hypoxia prevails as one of the limiting factors to achieve efficient O_2 -dependent therapies such as PDT [23] or RT [4]. Therefore, one of the strategies developed to re-oxygenate the tumor

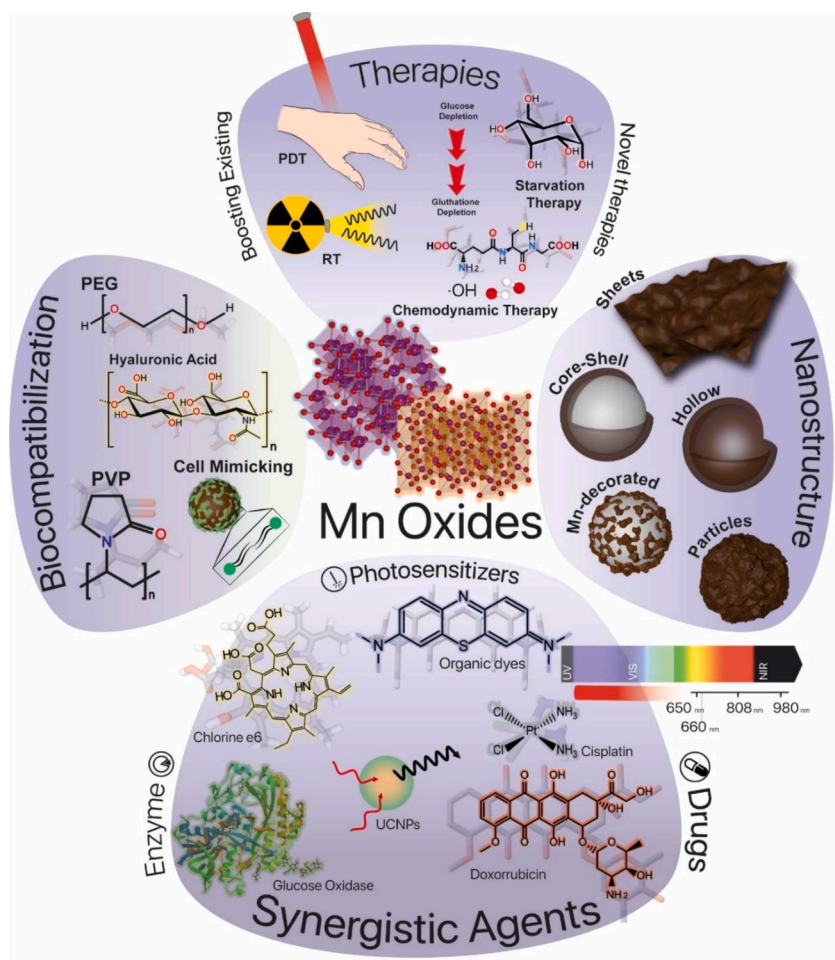


Fig. 2. Mn_xO_y nanoplatforms in cancer therapy. General overview of the main aspects explored in recent works that exploit the properties of Mn-based nanocatalysts in novel therapeutic approaches against cancer. Different Mn_xO_y morphologies have been employed including NSs [43], core-shell configurations [53], solid [67] or hollow [64] spheres, alone or in combination with other nanostructures. In addition, Mn_xO_y structures have been conjugated with organic polymers [67] or even with cell membranes or vesicles [72], to improve their biocompatibility and tumor targeting. Synergistic effects have been sought by combining Mn_xO_y with a variety of functional agents to increase anticancer effectiveness. These include enzymes such as GOx [66,67,69,72, 74]; PS (i.e. Chlorine e6 [63,75,76], methylene blue [77], porphyrins [78, 79]) or drugs (cisplatin [60] or doxorubicin [80]). These strategies endow Mn_xO_y nanoplatforms with multifunctional tools to tackle cancer via RT, PDT or starvation therapies (see Tables 1 and 2 and references therein).

Table 1Mn_xO_y nanomaterials employed as O₂-suppliers for combined cancer therapy, classified by different structural parameters and explored synergies for each material.

Nanohybrid	Mn _x O _y Morphology	Size (nm)	Bio-compatibilization	Other Synergies	Laser wavelength (nm)	Laser irradiance (W/cm ²)	Refs.
MnO ₂ - BSA ^a	Nanoparticle	15	BSA	–	–	–	[68]
MnO ₂ @UCNP	Nanosheet	–	–	PDT	980	2.0	[86]
Au@MnO ₂	Core-Shell	30;5	PEG (PAH-PAA-PEG)	RT	–	–	[62]
AuNCs@MnO ₂	Core-Shell	91	PEG600	PTT, CDT	808	0.80	[53]
MnO ₂ @Ce6	Nanoparticle	30	PEG (PAH-PAA-PEG)	PDT	661	5·10 ⁻³	[63]
MnO ₂ @ICG	Nanoparticle	239	–	PDT	808	0.50	[94]
SiO ₂ -MB@MnO ₂	Core-Shell	300;5	–	PDT	650	0.10	[77]
Hollow MnO ₂	Hollow	150	PEG (PAH-PAA-PEG)	PDT	660	5·10 ⁻³	[64]
MnO ₂ Nanodots	Nanodots	78.5; 6.8	–	CT, PDT	660	5·10 ⁻³	[88]
PtCo@MnO ₂	Nanoflowers	220	–	Oxidative stress	–	–	[103]
MON ^b @MnO ₂ @Porphyrin	Nanosheets	133.3	Organosilica	SDT	–	–	[79]
MnO ₂ -Ce6@UCNPs	Honeycomb	132	–	PDT	808	0.50	[109]
MnO ₂ @SPNsc	Nanosheets	50	PEG-b-PPG-b-PEG	PDT	808	0.44	[98]
PCM ^d @IR780@MnO ₂	Nanoparticle	140;1	Lecithin/DSPE	PDT	808	0.50	[90]
Fe ₃ C ₂ @GOx@MnO ₂	Core-Shell	24.1; 4.3	BSA	ST	–	–	[69]
MnO ₂ @GOx	Nanoparticle	36	RBC membrane	ST	–	–	[72]
Fe ₃ O ₄ @MnO ₂ @Ce6	Nanosheet	200	PEG	PDT	660	0.15	[75]
CD44@MnO ₂ @GOx	Nanoparticle	134.7; 15	Hyaluronic Acid	ST	–	–	[67]
MnO ₂ @BSA@IPI549	Nanoparticle	65	BSA	Immunotherapy	–	–	[70]
HMnO ₂ @LOX ^e	Hollow	65	RBC membrane	Metabolic/ Immunotherapy	–	–	[46]
MnO ₂ @WS ₂ @Fe ₃ O ₄ / sSiO ₂	Core-Shell	182	PEG (PAH-PAA-PEG)	RT	–	–	[65]
MnO ₂ /Cu ₂ -xS/siRNA	Nanosheets	200×1	PEG	PDT	980	0.72	[57]
¹³¹ I-HSA ^f -MnO ₂	Nanoparticle	40	HSA	RT	–	–	[110]
NCP ^g @Pt ^{IV} @MnO ₂	Nanoparticle	160	PEG	RT	–	–	[58]
MnO ₂ @DOX@BODIPY	Nanoparticle	74	PVP	CT, PDT	>600,	0.02	[89]
AgNC/Porphyrin/ MnO ₂	Nanosheet	200×1.5	–	PDT	635	1.0	[78]
MnO ₂ -Gox	Nanosheet	35×2	–	ST, PTT	808	1.0	[74]
MSNR ^h @MnO ₂ @Au	Core-Shell	200; 10	PVP	ST, RT	808	1.5	[101]
MnO ₂ @UCNP@DOTA ⁱ	Nanosheet	141.6	DOTA	CT	–	–	[111]
BP ^j -MnO ₂ -RhB	Nanoparticle	30	PEG-FA	PDT	660	0.15	[80]
UCNP@TiO ₂ @MnO ₂	Nanosheet	80; -	PEG5000-NH ₂	PDT	980	1.0	[59]
MnFe ₂ O ₄ @Ce6	Nanoparticle	390	mPEG-SG and mPEG-AM	PDT	680	0.50	[76]
BP-MnO ₂ -DOX	Nanosheet	110	–	PDT; PTT; CT	660	0.22	[112]
H-MnO ₂ -DOX-GOx	Nanoparticle	216	Hyaluronic Acid	CDT; PTT	808	0.94	[66]
Camptothecin@MnO ₂	Hollow	96.2	4T1 cell membrane	RT	–	–	[73]
Mn/PSAE ^k	Nanocube	270.0	DSPE-mPEG2K	PTT	808	1.5	[37]
BP@MnO ₂ @GOx	Nanosheet	275.0	–	PTT	808	1.0	[113]
MNP ^m @Ce6@MnO ₂	Nanoparticle	200.0	Hyaluronic Acid	PTT; PDT, CDT	808	0.64	[114]

^a BSA: Bovine Serum Albumin.^b MON: Mesoporous Organosilica Nanoparticles^c SPM: Semiconducting Polymer Nanoparticles.^d PCM: Phase Change Material.^e LOX: Lactate Oxidase.^f HSA: Human Serum Albumin.^g NCP: Nanoscale Coordination Polymer.^h MSNR: Mesoporous Silica NanoRod.ⁱ DOTA: Tretraazacyclododecane-1,4,7,10-tetraacetic Acid.^j BP: Black Phosphorous.^k PSAE: Pegylated Single Atom Enzyme.^m MNP: Melanin Nanoparticles.

PDT: Photodynamic Therapy, RT: Radiotherapy, CT: Chemotherapy, ST: Starvation Therapy SDT: Sonodynamic Therapy, PTT: photothermal therapy.

area consists in the decomposition of intratumoral H₂O₂, exploiting its overexpression in the TME [12–15], into O₂ together with the combination of a PS or a radiosensitizer to convert the as-generated O₂ into ROS to provoke cancer cell apoptosis. Catalases are highly efficient enzymes that yield O₂ from H₂O₂ decomposition following **Reaction 1**. Generally, a Fe atom present in the active site of the catalase natural enzyme breaks O—O bond in H₂O₂ which further evolves into O₂ [81]. Although the specific mechanism remains unclear, Mn centers in Mn_xO_y NPs can react with H₂O₂/H⁺ to produce O₂, according to **Reactions 2a–e** (as a function of the Mn stoichiometry), which perfectly fits with the TME conditions (H₂O₂ overproduction [12–15] and mildly-acidic

[16] conditions). This strategy is widely applied together with an O₂-consuming agent (as PSS) which transforms it into ROS to induce cancer cell apoptosis. This synergy confer Mn_xO_y-containing nano-platfoms with the ability to minimize the burdens of a hypoxic TME.



Reaction 1. H₂O₂ decomposition into O₂ and H₂O catalyzed by catalase enzyme.

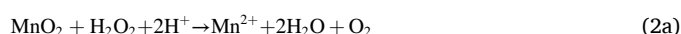
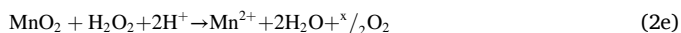
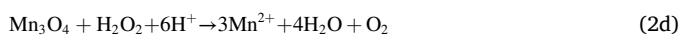
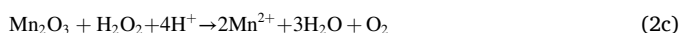
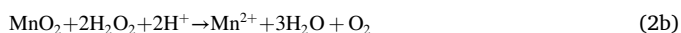


Table 2Mn_xO_y nanomaterials with different nanostructures reported in literature for the GSH-depletion strategy.

Nanohybrid	Mn _x O _y Morphology	Size (nm)(Large x width)	Surfaceligand	Other Synergies	Laser wavelength (nm)	Laser irradiance(W/cm ²)	Refs.
MnO ₂ @Ce6-DNAzyme	Nanosheet	(-)	-	PDT	-	-	[120]
MnO ₂ @Ce6	Nanosheet	80*	PEI	PDT	670	2.0	[121]
SiO ₂ @ MnO ₂	Core-Shell	80	PEG	CDT	-	-	[52]
SiO ₂ -Arg ^a MnO ₂	Core-Shell	59	(PAH-PAA-PEG) L-arginine	Induced Ferroptosis	-	-	[122]
UPCN ^b @SiO ₂ @MnO ₂	Core-Shell	53;2	PEG	PDT	650	0.5	[123]
MnO ₂	Nanosheet	255×2	Soybean Phospholipid	PTT	808	2.0	[50]
MON ^c @MnO ₂ @Porphyrin	Core-Shell	133	Organosilica	SDT	-	-	[79]
PCN-224@MnO ₂	Core-Shell	140	4T1 cell membrane	PDT	660	0.1	[124]
UPCN@MnO ₂ @Cisplatin	Nanorod, Core-Shell	47×33;5.1	PEG	PDT, CT	980	No data	[60]
MnO _x @OVAd@TFe	Nanospikes	-	-	CT	-	-	[129]
MnO ₂ @HMCuS ^f @DOX	Core-Shell	125;80	PEG	PTT	808	1.54	[61]
H-MnO ₂ -DOX-GOX-HA	Nanoparticles	216	Hyaluronic Acid	CDT; PTT	808	0.94	[66]
Zn _x Mn _{1-x} S ₈ @PDA	Hollow	300	Polydopamine	CDT, PTT	808	2.0	[126]
Au-MnO ₂	Janus	100	PEG	CDT, RT;	-	-	[130]
MCMnH	Nanoparticle	200	Hyaluronic Acid	PTT; PDT, CDT	808	0.64	[114]
Au@H-MnO ₂	Janus	200	-	CDT	-	-	[131]

^a Arg: arginine.^b UCNP: UpConverting Nanoparticle.^c SPN: Semiconducting Polymer Nanoparticles^dOVA: Ovalbumin^eTF: Tumor-fragment membrane.^f HMCuS: Hollow Mesoporous Copper Sulfide.

Reactions 2a-2e. Redox reaction between Mn_xO_y with H₂O₂ to produce O₂, mimicking natural catalase activity, with stoichiometry variations as a function of the oxidation state of the starting Mn_xO_y enzyme-mimicking surrogate.

Based on the literature reports in cancer therapy, we propose the mechanism depicted in Fig. 3a where H₂O₂ donates 2e⁻ to the electrophilic Mn⁴⁺ group. Mn-based nanostructures reported for cancer therapy possess an amorphous structure with Mn-O bonds susceptible to breakage as H₂O₂ donate its π_p^{*} electron density to antibonding e_g^{*} orbitals of Mn⁴⁺. A peroxo-Mn³⁺ intermediate that further evolves into O₂ in H₂O media is reported in literature [82,83] The resulting Mn²⁺ center possess fast H₂O exchange kinetics [84] and the subsequent dissolution in Mn(H₂O)₆²⁺ takes place at the end of the process. Previous literature reports endorse the O₂-generation activity of MnO₂ nanomaterials with poor Mn²⁺ lixiviation at pH=7.4, but quite higher at mildly-acid pH [85, 86]. This may be attributed to higher OH⁻ concentrations and further coordination with the Mn³⁺ center, avoiding H₂O exchange. Kinetic studies of H₂O₂ decomposition into O₂ catalyzed by MnO₂ reveal a fast evolution over time (*k* = 0.074 min⁻¹, pH = 7.0) [87], which suggest a fast reoxygenation of tumor cells in the presence of MnO₂. Several studies *ex vitro* [46,71,74,88,89] demonstrate an immediate fast O₂ production in presence of MnO₂/H₂O₂ system, accentuated by higher H⁺ concentrations [89] or external stimuli as light irradiation [90]. Regarding the influence in morphology, Singh et al. [91]. provided clear insights comparing the activity of different Mn₃O₄ nanostructures, being nanoflowers the most active morphology (*V*_{max} = 7.324·10³ μM·s⁻¹) followed by nanoflakes (*V*_{max} = 1.305·10³ μM·s⁻¹) and finally hexagonal plates, polyhedrons and cubes, with analogous activity. This reactivity trend is explained by two important insights: (i) nanoflowers and then, nanoflakes, possess larger surface area where many active sites may

decompose H₂O₂ into O₂ [92] and (ii) higher electrical conductivities directly correlate with larger redox activities. In their study, they also compared the potential influence of Mn oxidation states (Mn₃O₄, MnO₂, Mn and Mn₂O₃) [91]. Mn₃O₄ exhibited much higher activity in comparison to the other Mn oxides, indicating the relevance of mixed valence states (Mn²⁺ and Mn³⁺) simultaneously present in the nanostructure.

Moreover, the synthetic versatility of Mn_xO_y enables the combination with O₂-dependent active agents, such as PSS, i.e. chloride e6 [63, 75,76], porphyrins [78], or other pigments as indocyanine green (ICG) [94] or methylene blue (MB) [77] or enzymes widely employed in cancer therapy such as GOx [66,69,72,74] to achieve an even more effective treatment (listed in Table 1). As a result, Mn_xO_y nanosystems have been recently explored as catalase-surrogates (Fig. 3). Prasad et al. [68]. and their pioneering work with BSA (Bovine Serum Albumin) functionalized MnO₂ nanoparticles demonstrated their capacity to *in situ* generate O₂ and overcome the burdening tumor hypoxia following the process described in Fig. 3a. Moreover, the rich surface chemistry of MnO₂ NPs enabled the proper interaction with BSA to increase stability in cell media and reduce their potential cytotoxicity. PDT has also emerged as an alternative cancer treatment consisting in the light irradiation of a tumor typically in the Near Infrared (NIR) window (due to its high skin penetrability and limited absorption by tissue and organelles [95]) which interacts with a responsive PS [23,96] or optically responsive NPs [86,97]. Typically, the energy of excited PS is transferred to O₂ in order to produce ROS that damage key molecules in cell, such as DNA or proteins, entailing cell apoptosis and death [20]. The synergetic combination of PDT with the *in situ* O₂ production from H₂O₂/H⁺ present in tumors has been successfully exploited in the recent years taking advantage of the O₂-production capabilities observed in MnO₂ NPs [24,33] and illustrated in Fig. 3b.

This concept was further developed by Zhu et al. [63] with a biocompatible nanoplatform combining MnO₂ nanoparticles and a PS (Ce6) active in the red window (λ_{abs} = 661 nm). The biocompatibility process was carried out with polyethylene glycol (PEG) to enhance stability and dispersity. MnO₂ NPs were synthesized combining the use of permanganate and Polyacrylic acid (PAH) as reducing and stabilizer polymer [68]. After introducing Ce6, the nanoplatform was coated with

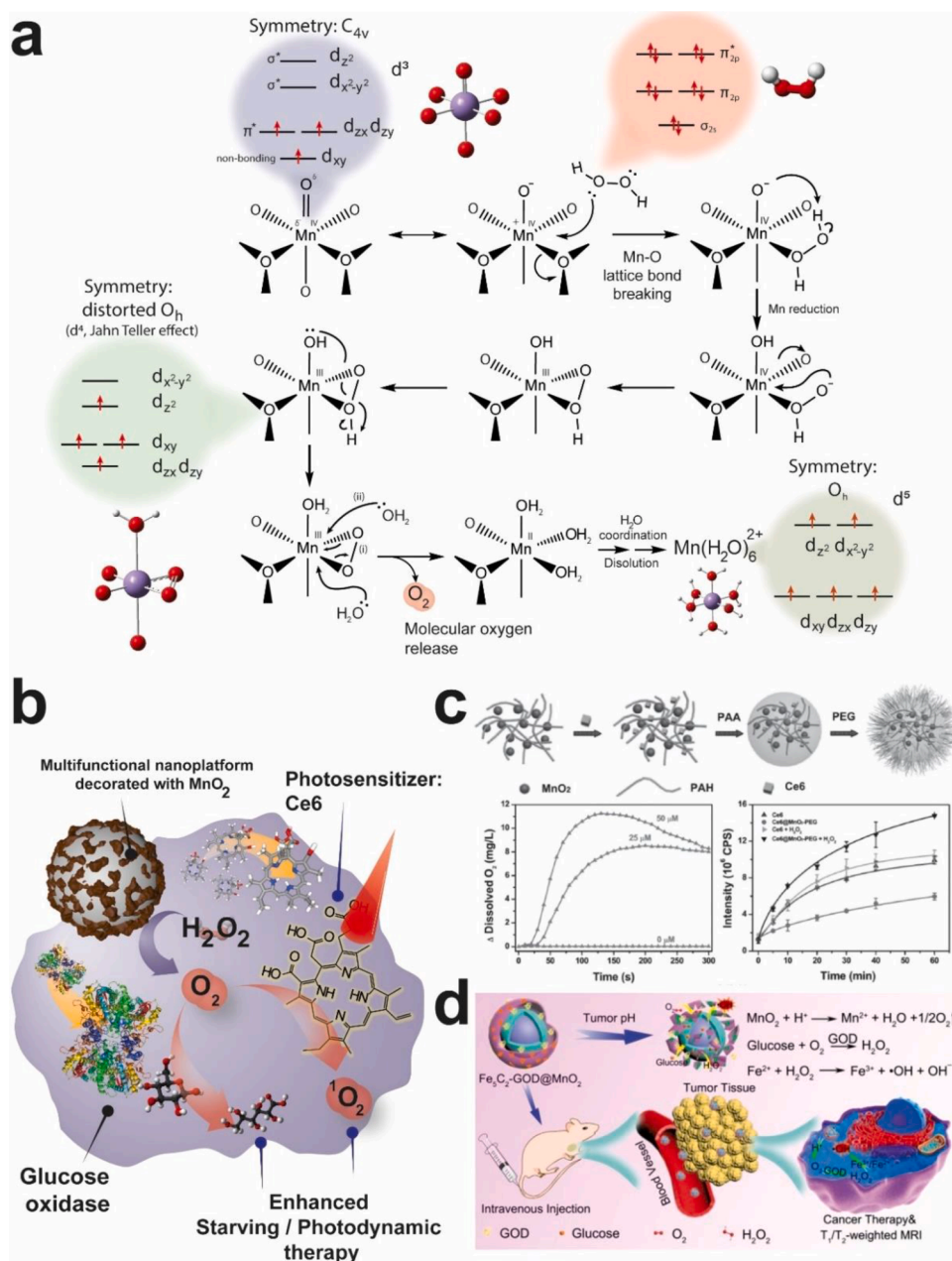


Fig. 3. O_2 -generation activity of Mn_xO_y nano-materials and their application in cancer therapy. (a) Reaction mechanism describing the generation of O_2 retrieved from H_2O_2 onto a Mn_xO_y surface; Oxo groups on MnO_2 surface are responsible for reacting with H_2O_2 , yielding a $MnOOH$ intermediate. The influence of the reaction environment drives two different paths: either a concomitant reaction with H_2O_2 to yield another molecule O_2 , or a direct reaction with H^+ to produce H_2O molecules [93]; (b) Schematic representation of the O_2 -producing activity of Mn-oxides nanosystems. O_2 enhanced production from H_2O_2/H^+ assisted by MnO_2 nanocatalysts maximizes the effectivity of O-dependent therapies such as PDT that require the presence of O_2 to favor the subsequent generation of ROS upon visible-NIR photoexcitation of an organic sensitizer such as Ce6; (c) O_2 -generation for a MnO_2 -containing nanomedicine and its implications regarding light triggered generation of 1O_2 using Ce6 as PS. Reproduced with permission from [63], Copyright 2016, Wiley-VHC; (d) Synergistic enzymatic glucose degradation and MnO_2 -assisted O_2 production through cascade reaction to perform starving therapy. Reproduced with permission from [69], Copyright, 2018, American Chemical Society.

Polyacrylic Acid (PAA) through layer by layer (LBL) method and subsequently treated with NH_2 -PEG to achieve the final and stable product (Fig. 4c). *In vitro* studies revealed an *in-situ* increase of O_2 concentration levels from 0 to 11 mg L^{-1} in the presence of $50 \mu\text{M}$ of $MnO_2@Ce6$ and 10 mM of H_2O_2 after 2.5 min. Moreover, there was an outstanding difference in the levels of singlet oxygen (1O_2) derived from O_2 upon irradiation with red light at 661 nm light and in the presence of both PS and H_2O_2 . The efficacy of this strategy at *in vitro* studies was confirmed using an inert N_2 ambient in the cell culture [63]. Large differences regarding the cell viability after the laser irradiation treatment were found in comparison to free Ce6 under N_2 atmosphere due to the scarcity of intracellular O_2 . Finally, *in vivo* studies revealed a significant tumor size reduction when Ce6@ MnO_2 -PEG was injected and 1 h of laser irradiation was applied. In contrast, this O_2 -producing behavior was not observed in the absence of MnO_2 nanoparticles (highlighted in Fig. 3c).

Likewise different Mn-based nanoarchitectures loaded with Ce6, such as MnO_2 nanoflowers [75], hollow MnO_2 nanospheres [64] or hybrid structures [72,88] led to analogous successful outcomes.

Interestingly, it was also observed that the O_2 -producing activity of the MnO_2 NPs could be combined with other photosensitizing candidates such as ICG [94], MB [77] or semiconducting organic NPs [98] to enhance the PDT performance (see also Table 1). Likewise, MnO_2 nanoparticles have been also combined with up-converting Nanoparticles (UCNPs), which can absorb two or more incident photons with lower energy (i.e. higher wavelengths) and emit a single one of higher energy (i.e. lower wavelength) [99]. One of drawbacks associated to PDT lies on the limited irradiation energies allowed for treatment. This restriction withholds the yield and number of PS reliable candidates to be efficiently used beyond UV and visible ranges. Somehow, the use of UCNPs and NIR light can alternatively compensate the action of PS and still generate UV-visible photons inside the tumor cell for a more effective therapy [100]. Fan et al. [86] fabricated a nanoplatform based on $NaYF_4:Yb(18\%)/Er(2\%)/Tm(1\%)$ up-converting core, a PS-containing shell made of SiO_2 to avoid PS leaching and a MnO_2 sheet surrounding various core-shell NPs. The generation of singlet oxygen species (1O_2 derived from O_2 , see Fig. 3b) was confirmed and attributed

to an energy transfer from the Mn core to the PS after excitation with a NIR source. The simultaneous presence of H₂O₂ and MnO₂ induced the *in situ* generation of additional O₂ that led to an enhanced production of ¹O₂ species (see Fig. 3b). Moreover, mild acidic conditions additionally ensured H⁺ levels to yield O₂ via Reactions 2a. Finally, the researchers analyzed the expression of Hypoxia Induced Factor (HIF) in tumor tissue whose degradation depends on O₂ levels [86]. The treatment with the MnO₂-containing nanoplatform showed a remarkable down-expression of HIF-1 α , demonstrating its capacity of generate O₂ inside the tumor.

The potential benefits of remotely triggering a localized O₂ supply within a tumor environments has also attracted the attention of other cancer therapies aimed at targeting the depletion of nutrients inside tumor cells, especially glucose [8], to alter the metabolism and tumor growth [26]. In this regard, GOx natural enzymes have been tested for starvation therapy purposes due to its selectivity and efficiency towards glucose conversion into gluconic acid [27]. The enzymatic reaction of GOx provides H₂O₂ and gluconic acid (which increase H⁺ in the medium) as by-product requires of O₂ as a reactant, which is a limitation in tumor cells due to their hypoxic state. This represents an ideal scenario for the complementary role of Mn_xO_y nanoparticles to facilitate additional O₂ supply in the catalytic glucose oxidation cycle (see further details on Fig. 3b).

Feng et al. exploited this concept [69] through the functionalization of Fe₃C₂ cluster-like centers with GOx physically adsorbed, and adding a MnO₂ shell after KMnO₄ reduction (Fig. 3d). MnO₂ shell boosted O₂ levels inside the tumor and exhibited a good synergy with both GOx and Fe₃C₂ thereby enhancing glucose depletion and further ROS production through Fenton-like reaction of Fe₃C₂. Moreover, the Fe-based core allowed a delivery of the nanoplatform *in vivo* to the tumor with the aid of directing magnets. Remarkable differences to stop the tumor development were achieved in comparison to the nanoplatform alone. GOx and MnO₂ systems have been also tested in combination with the PDT sensitizer Ce6 by Yang group [72]. MnO₂ nanoparticles and GOx were bioconjugated with BSA to avoid further aggregation and maximize biocompatibility. *In vitro* results showed both glucose oxidation and ROS production enhanced by the presence of MnO₂ in comparison with GOx and Ce6 alone, remarking the O₂-production of MnO₂. Confocal microscopy studies demonstrated the capability of the entire nanoplatform to generate ROS under laser irradiation *in vitro* in a 1% O₂ atmosphere, resulting ideal candidates to overcome TME hypoxic levels while producing ROS. Tissue analysis of the HIF-1 α after the NPs injection corroborated the capacity of the MnO₂ in the relief the intratumoral hypoxia (Fig. 3d). Finally, not only their combination with natural GOx has been effective, Yang et al. [101] demonstrated the successful supply of O₂ from MnO₂ to a GOx-like nanozyme, AuNPs, to enhance starving/radiotherapy in the same way as described before. RT is also a therapeutic approach based on the transformation of O₂ into ROS where the chemistry of MnO₂ may play interesting synergies. Yi et al. [62] synthesized AuNPs@MnO₂ core-shell nanostructures for application in RT. Au NPs have been widely used as RT agents due to Au interaction with X-rays [102] to induce cell death but exhibit limitations in hypoxic environments. MnO₂ shell display O₂-generating activity to overcome hypoxic-cell state and enhance RT efficacy. In addition, other metallic nanostructures were combined with MnO₂ to achieve higher therapeutic efficiencies. Pt-Co nanoflowers developed by Wang et al. [103] showed intrinsic oxidase-like activity to induce oxidative stress to cancer cells, transforming molecular O₂ into reactive \bullet O₂⁻ species. By loading them with MnO₂ NPs, the chemical behavior of MnO₂ *in situ* supplied enough O₂ to PtCo (under a pH range from 5.0 to 7.4) to ensure high ROS levels and induce cell death.

The O₂-generating capabilities of MnO₂ and the subsequent depletion of HIF-1 α has also been exploited by immunotherapy. T-cells from immune system are capable of recognizing and killing cancer cells but this process is blocked by the interaction between inhibition checkpoint molecules, as Programmed Cell Death-Protein (PD-1) [104] and its ligand PD-L1 [105]. Thus, many tumors overexpress PD-L1 to avoid

immune system reducing the potential outcome of immunotherapy [47]. Since the expression of HIF-1 α upregulates PD-L1, the generation of O₂ by MnO₂ within the TME may establish quite favorable synergies with immunotherapeutic agents [106]. In this context, Yu et al. [70] developed a nanoplatform containing MnO₂ and IPI549, a potent inhibitor of PI3K γ -pathway, which potentially promote tumor migration and reduces production of inflammatory mediators to avoid immune system. This synergy achieved a reduction three times larger of the tumor (4T1 cells) in comparison with using only IPI549. The hypoxic tumor microenvironment can also promote the accumulation of regulatory T cells (reg-T) and M2 type Tumor Associated Macrophages (TAM) [107], which are immunosuppressive cells that favors tumor progression [108]. Yang et al. [64] found out that 4T1-tumor treatment with a MnO₂-Ce6@DOX nanoplatform not only enhanced tumor suppression due to the synergy between O₂ generation-consumption displayed by the system MnO₂-Ce6, but also promoted polarization of M2-TAM to M1 and the downregulation of reg-T within tumor. Further on, the combination of this effect provided by MnO₂-Ce6-DOX with anti-PD-L1 checkpoint blockade yielded promising results whether in primary and distant 4T1-tumors.

In summary, a panoply of strategies for cancer therapy are focused in transforming endogenous O₂ into ROS to provoke cell apoptosis. The hypoxic conditions displayed by TME hinders the therapeutic outcome of mentioned treatments. Chemical reaction triggered by MnO₂ nanostructures with intratumoral H₂O₂ to form O₂ and overcome tumoral hypoxia has been widely exploited by different therapies (i.e. PDT, RT, ST, SDT) with promising results, highlighting the strong potential of MnO₂-containing nanomedicines as anticancer agents.

3. Glutathione depletion strategies by Mn_xO_y nanostructures

Along with the O₂ scarcity, another limitation provided by TME for current cancer therapies consists in the overexpression of antioxidants, concretely GSH [17–19,115]. GSH is considered to be a source of resistance in CT [116] and RT [117] and thereby its depletion by Mn_xO_y is a current strategy to improve the efficacy of these therapies. Cells can generate H₂O₂ and other ROS under different circumstances, such as cellular respiration or fatty acid oxidation [118]. However, cells also possess different mechanisms to counteract the detrimental effects of these species to minimize damages. GSH is the main antioxidant in animal cells and maintains ROS levels below cytotoxic levels, following Fig. 4a [18]. In this process, two molecules of GSH can transform one molecule of H₂O₂ into innocuous H₂O with the aid of glutathione peroxidase (GPX4) enzyme [19,115,118].

Continue oxidative stress [11] entails GSH overexpression in cancer cells [17,18], which limits the effectivity of some ROS-based treatments. From the therapeutic point of view, GSH depletion in cancer cells blocks one of their defense mechanisms against ROS and promotes cell apoptosis and death [119]. Therefore, the oxidant capabilities of Mn_xO_y nanostructures and the mildly acidic conditions in TME represent two appealing scenarios to promote the successful GSH depletion following Reactions 3 (vide infra) [24]. A wide range of Mn-based nanostructures, including nanosheets [50,120,121] core-shell [52,60,61,79,122–124] were recently tested as GSH-removal inorganic candidates. These strategies focused on GSH depletion are exploited with the co-adjuvant role of other functional agents to perform on different therapeutic strategies as summarized in Table 2. Regarding the effect of MnO₂ in remove GSH and its implications in ROS enhancement, Fan et al. [121] proved the influence of 1–10 mM GSH concentrations [125] and their ability to deplete the ¹O₂ generated by Ce6 under NIR radiation.



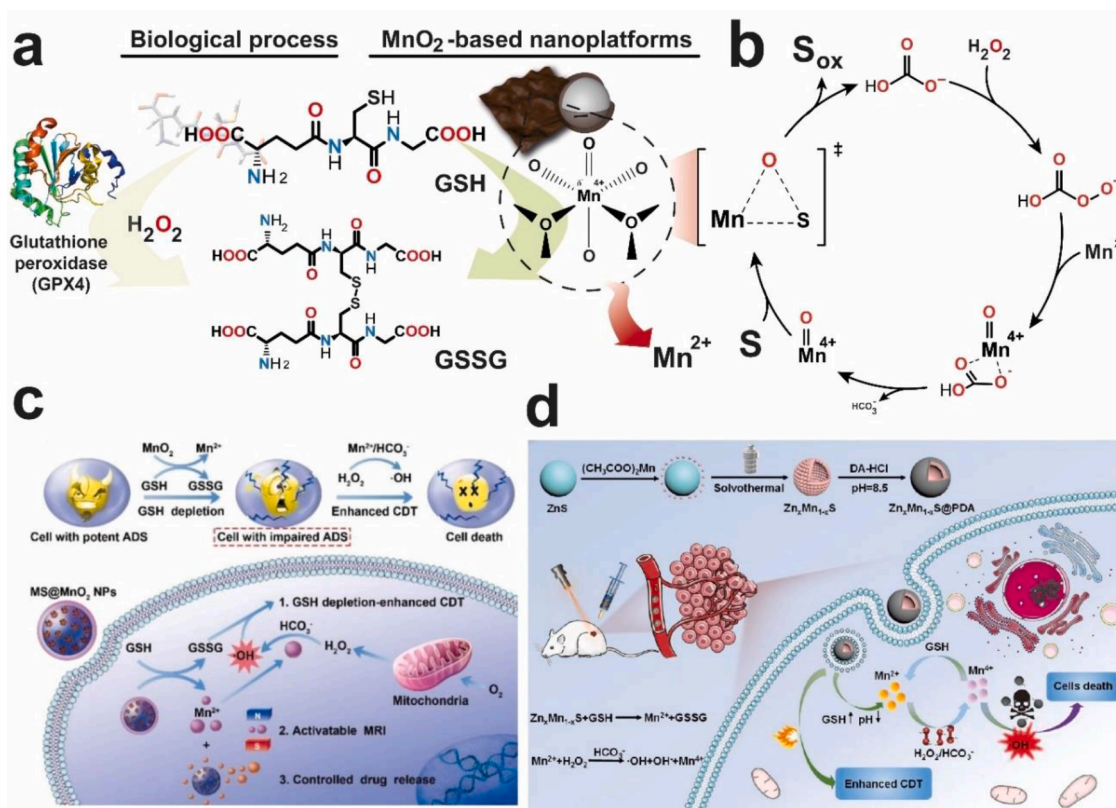


Fig. 4. Biological and chemical interaction of GSH with MnO_2 nanomaterials. (a) Natural depletion of H_2O_2 and GSH catalyzed by GPX4. The chemical structures of GSH and oxidized GSH are shown. Thiol (-SH) in GSH is the active group in H_2O_2 reduction and yields the final GSSG dimer; (b) The generated Mn^{2+} ionic species can react with the excess of H_2O_2 to oxidize organic molecules. Mn^{2+} -catalyzed oxidation of organic substrates via (OH)(O)COO⁻ intermediates. In a first step, H_2O_2 oxidizes (OH)(O)COO⁻ yielding the peracetic acid intermediate which can further oxidize Mn^{2+} to produce the highly oxidative Mn-oxo-O species. Finally, the coordination of an organic substrate to Mn-oxo-O, facilitates the oxygen transfer to yield the final oxidized product [44]; (c-d) Different Mn-containing nanoplateforms which perform the proposed reaction cascade. Firstly, Mn^{IV} center react with GSH to yield GSSG and Mn^{2+} , respectively. Generated Mn^{2+} are able to react with endogenous H_2O_2 , aided by present HCO_3^- , to promote $\bullet\text{OH}$ species for inducing cell apoptosis. Reproduced with permission from [52], Copyright 2017, Wiley-VHC. Reproduced with permission from [126], Copyright 2021, American Chemical Society.

Reactions 3a-c. Different Mn-oxides reactions with GSH to yield oxidized GSSG.

They constructed a MnO_2 -Ce6 nanosystem with the capability of depleting overexpressed GSH from cancer cells by redox reaction with MnO_2 and $^1\text{O}_2$ production through NIR radiation and Ce6. In comparison with free Ce6, MnO_2 @Ce6 demonstrated a more effective PDT due to the synergistic removal of GSH. However, MnO_2 possess not only the ability to react with GSH, but also in the presence of H_2O_2 and biological $\text{HCO}_3^-/\text{CO}_2$ buffer [52] following the mechanism illustrated in Fig. 4b. GSH interaction with MnO_2 and the further production of $\bullet\text{OH}$ was firstly investigated by Lin et al. [52] (Fig. 4c). After the dissolution of MnO_2 triggered by GSH, the released Mn^{2+} ions can react with pre-formed percarbonate ions to yield oxidizing Mn-oxo species. Such this reactive product can further react with an organic substrate, achieving its final oxidation. The homogeneous mechanism presented in Fig. 5b was approached by Ember et al. [44] and has been widely accepted in literature concerning Mn^{2+} ions and Fenton-like activity (Fig. 4d).

In terms of reaction kinetics, several works study the Mn^{2+} releasing profile of Mn_xO_y nanostructures as a product of their reaction with GSH or mildly acidic media (pH = 5.5–7) [60,75,122,123]. Following Xu and co-workers investigation [123], the favorable chemical conditions that tumoral chemistry provides ensures a fast MnO_2 degradation into Mn^{2+} ions (100% in 1 h), while in normal tissue conditions (low GSH and H_2O_2 concentrations and pH close to 7.4) the degradation is much slower (<10% in 1 h). These strategies aimed at using the as-generated Mn^{2+} as Fenton-like catalyst, generating toxic ROS species following mechanism depicted in Fig. 4b [52,127,128]. Nevertheless, the mechanism is still

under debate. MnO_2 can induce oxidative stress in cell by two different mechanisms: removing antioxidant species and generating excess ROS toxic substances. Moreover, high GSH concentrations burden/limit/reduce/have a negative impact the action of anticancer drugs like Doxorubicin (DOX) [122] or cisplatin [60]. Consequently, the combination of these anticancer drugs or other therapies such as immunotherapy [96], PDT [60,61,120,121,123,124], SDT [79] or CT [60] with the GSH-depletion action of MnO_2 represents a promising synergistic effort to boost the effectiveness of the therapy treatments (Fig. 2).

4. The fate of Mn^{2+} released from nanoparticles in the cell environment

4.1. Mn_xO_y nanoarchitectures as Mn^{2+} reservoirs

As pointed out in the previous section, one of the reaction products between Mn_xO_y and H^+ /GSH are Mn^{2+} ions (see reactions 3a-3c). These Mn-containing nanostructures can be understood as “Mn-reservoirs” which will dissolve into Mn^{2+} under reductive environments such as TME. These Mn^{2+} species will display key catalytic activities within the TME (overall in Fenton-like processes) and may enter into metabolic pathways where Mn is involved. Up to now, several papers [46,60,74,75,88,89,122,123] where kinetics of Mn_xO_y NPs with H_2O_2 /GSH environments are described, use amorphous [75,88,122,123] or poorly crystalline structures [74,89]. A disordered and poorly-aligned structure entails a weakening of Mn-O σ bond due to an unfavorable orbital overlapping [132], enables the interaction of Mn with π^* orbitals of

H_2O_2 or GSH and leads to the consequent Mn^{2+} dissolution [133] (Fig. 5a).

A production of Mn^{2+} ions will be thermodynamically favored, as electrons from $\text{H}_2\text{O}_2/\text{GSH}$ are injected in e_g^* antibonding orbitals and Mn^{2+} is the favorable oxidation state in tumor pH-range following Pourbaix diagram, depicted in Fig. 1b. Consequently, although extracellular H_2O_2 and GSH concentrations are low [134,135], other reducing agents as Serum Albumin [136] can affect the Mn_xO_y stability prior to its cell internalization. A deeper and systematic research in the effect of crystallinity in Mn^{2+} releasing kinetics is necessary to reach a major control in the administration of Mn_xO_y based nanomedicines and know the potential degradation outside cancer cell Mn_xO_y materials can suffer. Strategies followed in current cancer-therapy research using Mn_xO_y aim for *in situ* generation of O_2 and GSH depletion. Several works conclude that the appearance of Mn^{2+} species will generate highly reactive hydroxyl radicals $\bullet\text{OH}$ ($E^0=2.8$ V) through a Fenton-like reaction in the presence of $\text{H}_2\text{O}_2/\text{HCO}_3^-$. Reduction potential of $\text{Mn}^{3+}/\text{Mn}^{2+}$ is 1.51 V, which means that removing an electron from Mn^{2+} in a hexaqua complex is a highly energetic process and redox-mediated catalysis is not feasible. Nevertheless, the cell is a molecule-rich environment and the formation of diverse and unknown Mn^{2+} complexes with interesting catalytic properties is favored. Following ligand field theory,

the complexation to Mn^{2+} with strong π -donor ligands such as HCO_3^- (or even carboxylic groups in biomolecules as glycine, citrate...) affect to the energetic value of e_g^* and t_{2g} orbitals, lowering the $E_{\text{Mn}^{3+}/\text{Mn}^{2+}}$ [137] (Fig. 5b).

Following other Fenton-like reaction pathways with Fe and Cu, the production of $\bullet\text{OH}$ occurs when the reduced metal (i.e. Fe^{2+} and Cu^+) reacts with H_2O_2 , yielding $\bullet\text{OH}$ and the oxidized metal [138,139]. In the particular case of Fe^{3+} , the reduction to regenerate the active Fe^{2+} center is usually the Rate Determining Step (RDS) as the reaction kinetics are considerably lower in comparison with the first reaction [138]. In the case of Mn^{2+} the opposite situation occurs. The presence of a donor ligand, such as HCO_3^- enables the reaction of Mn^{2+} with H_2O_2 by: (i) lowering the energy of electronic transferences from H_2O_2 to Mn^{2+} and (ii) allowing H_2O_2 -mediated oxidative catalytic cycles efficiently yielding $\bullet\text{OH}$ (Fig. 5b). This has been recently highlighted by Meng et al. [140], who determined the relevance of $\text{Mn}^{2+}(\text{HCO}_3^-)$ complex in oxidation reactions for $\text{Mn}^{2+}-\text{H}_2\text{O}_2-\text{HCO}_3^-$ system. However, classical homogeneous catalysis concepts have not been transferred to nanobiomedicine yet. Ember et al. [141] demonstrated the relevance of the substrate in $\text{Mn}^{2+}/\text{HCO}_3^-/\text{H}_2\text{O}_2$ system, stabilizing *in situ* formed reaction intermediates. Oxidation rate of substrates depends on their electron-donor capability to stabilize Mn^{2+} . The immediate question is

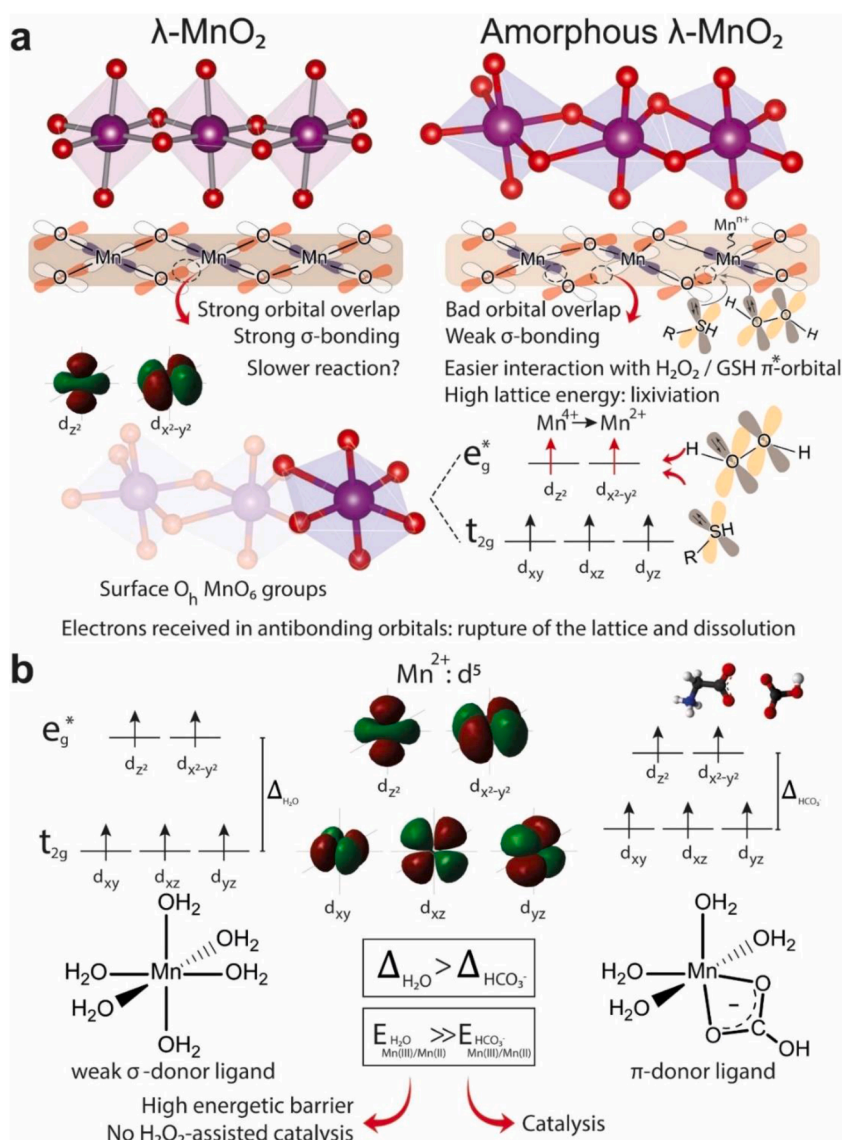


Fig. 5. (a) Differences in the lattice between crystalline and amorphous MnO_2 : disordered dispositions derived from amorphous structures forms high-energy local sites due to poor molecular orbital alignment. This fact facilitates the interaction with key cancer metabolites as GSH or H_2O_2 to promote Mn^{2+} and keep with the reaction cascade with $\text{H}_2\text{O}_2/\text{HCO}_3^-$. (b) Formation of Mn^{2+} -coordination complexes with present HCO_3^- in physiological media. The strong donation of π -electronic density, stabilize e_g^* orbitals of Mn^{2+} and provoke an easier oxidation to Mn^{3+} to sustain the redox catalytic cycle with H_2O_2 . This electronic stabilization enables a suitable $E^0_{\text{Mn}^{2+}/\text{Mn}^{3+}}$ to perform redox-catalysis and oxidize organic compounds in TME through $\bullet\text{OH}$ production.

whether the preferential oxidation of a type of molecules when Mn^{2+} is introduced in a cell is taking place, and if it is possible to achieve some selectivity with electron donor molecules and key cancer cell metabolites such as glucose, cofactors or aminoacids.

Among the wide variety of Mn oxidation states (from Mn^{2+} up to Mn^{7+}), only three of them are present within the cell environment (Mn^{2+} , Mn^{3+} and Mn^{4+}) (see Fig. 1b). The first of them, Mn^{2+} , in spite of presenting stability due to its d5 electronic configuration, exhibits lower affinity to oxygen and nitrogen ligands than Fe^{2+} and Zn^{2+} . In addition, Mn^{2+} centers exhibit a very rapid ligand exchange kinetics and can be easily replaced by other ions, such as Mg^{2+} . The second one, Mn^{3+} is a powerful oxidizing agent, due to its empty d orbital. It is known that, under aerobic conditions at neutral pH, hydrated Mn^{2+} ions are stable in water. However, under basic conditions it is easier to oxidize Mn^{2+} to Mn^{3+} , due to the possibility for a metal-bound water molecule to lose a proton and yield a hydroxide ligand (which stabilizes the charge of the Mn^{3+}). In case this charge increases, the pK_a of a second water ligand is reduced causing the oxidation of Mn^{3+} species into Mn^{4+} , which can precipitate as solid MnO_2 . Mn oxidation states need to be controlled within enzymes by the protein environment so that unwanted side reactions are avoided [142].

4.2. Trafficking and redox chemistry of Mn-based systems at the intracellular level

The Mn^{2+} released from the Mn-containing nanoplateforms can enter inside the traffic routes of biological Mn which of course will have potential effects and must be considered regarding a future clinical translation of Mn-based nanomedicines. While, in general, Mn deficiency is not a widespread situation, it is reported that extended exposure to this metal mainly causes its accumulation in kidney, bone, liver, pancreas, and brain, which is the primary target tissue of Mn toxicity [143]. Chronic exposure to Mn is also known to affect the central nervous system (CNS) [144] and continuous low-level exposure to Mn in rats has proven to cause neuronal oxidative stress, mitochondrial damage, protein aggregation and misfolding, endoplasmic reticulum stress, autophagy dysregulation and apoptosis [143,145]. *In vitro* toxicity studies allow to compare cytotoxicity of different NPs showing that Mn_xO_y NPs and ionic Mn^{2+} -based NPs display lower toxicities than other NPs based on Mo or Ag in PC-12 cells lines [146]. Thus, the biological importance of Mn lies on its dual role as both a nutrient and a toxic element. As a consequence, not only uptake and trafficking of this ion must be controlled, but also its secretion [147]. Generally, most of excess of Mn is managed via liver and conjugated to bile to be eliminated as fecal excretion [143].

Mn-dependent activity is ubiquitous in cells. Thus, organisms must have mechanisms in order to transport, detoxify, sequester and eliminate this metal so that Mn homeostasis is maintained. Different

homeostasis proteins are involved in this mission, including cell surface and intracellular Mn transporters, and Mn chaperones [147]. As can be seen in Fig. 6a, under normal physiological conditions and complete availability of Mn, both uptake and intracellular dissemination of the metal depend on two natural resistance-associated macrophage protein (NRAMP) Mn transporters. The first one, NRAMP1, is located in the cell membrane and transports Mn^{2+} into cytosol. The second one, NRAMP2, present in intracellular Golgi-like vesicles, is responsible for transporting Mn from the cytosol to the Golgi, where the transporting ATPase Pmr1p delivers Mn to sugar transferases (Stase), or to mitochondria to be used by superoxide dismutase 2 (SOD2) by the action of another transporter called, Mtm1p [147]. In the case of cells exposed to elevated levels of Mn, as in the case of Mn_xO_y NPs, the NRAMP transporters are barely expressed. However, Mn can still be bio-accumulated by the generation of Mn-phosphate complexes taken up by the Pho84p phosphate transporter. In that case, other proteins known as SPCA1 and SPCA2 internalize Mn in vacuoles for elimination. This clearance pathway (Fig. 6b) plays an extremely important role in Mn homeostasis and detoxification, taking into account the toxicity related to high Mn concentrations [142, 147]. Therefore, the way this Mn homeostasis is altered directly affects tumor cell status. Thus, altering the cell metabolic capability through Mn could be an interesting strategy in order to burden tumor growth. Apart from SOD2 and Stase, different Mn-dependent enzymes need to be synthesized by the cell. They take advantage, as previously described, of Mn oxidation states so that its redox properties allow the important catalytic diversity demanded in the cytosol [142].

4.3. Mn^{2+} favors antitumor immune response

The presence of DNA in the cytosol is associated with a potentially harmful scenario for cells (tumorigenesis, viral infection or presence of bacteria) [148]. cGAS-STING pathway is a component of the immune system whose task is detecting cytosolic DNA and trigger a response for activating defense mechanisms. Jiang group recently provided with valuable insights in the activation of cGAS-STING pathway for host defense against cytosolic DNA promoted by the presence of Mn^{2+} ions [149]. In a follow-up work, they demonstrated that Mn^{2+} upregulates cGAS-STING pathway to provoke antitumor immune responses, concretely via CD8+ T and NK cell activation [47]. Further on, they proved how a combinatory therapy using anti-PD-1 antibody and $MnCl_2$ supplementation resulted in significant B16F10 tumor reduction due to the activation of immune system. Considering the potential production of Mn^{2+} ions inside tumor cells upon treatment with MnO_2 nanostructures, a wide range of synergies with immunotherapeutic agents may be established to boost antitumor immune response.

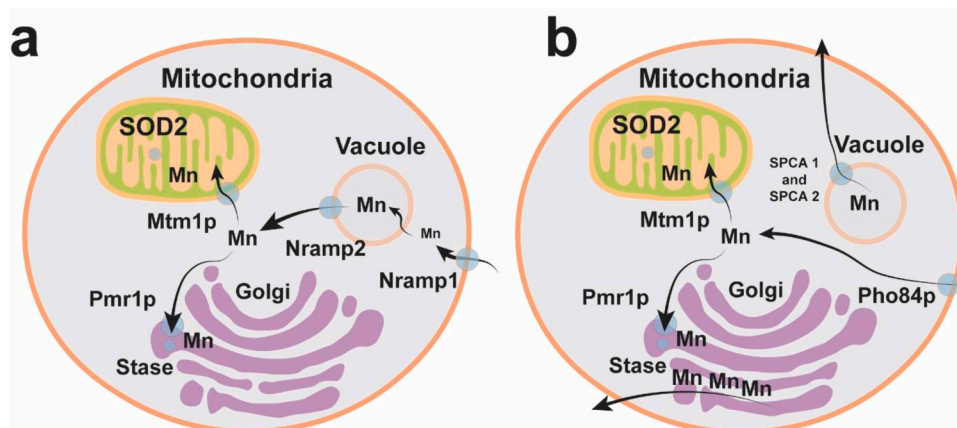


Fig. 6. Mn intracellular trafficking and redox potentials of Mn_xO_y materials. (A) Intracellular trafficking scheme of Mn under normal physiological growth conditions: (i) Mn is taken up via the NRAMP1 transporter at the cell surface; (ii) Mn is transported by NRAMP2 to either the Golgi or mitochondria; (iii) Pmr1p pumps Mn into the Golgi for activation of Stase, while Mtm1p helps Mn transport into mitochondrial SOD2; (B) Intracellular trafficking scheme of Mn under high concentration conditions: (i) Nramp transporters are not significantly expressed; (ii) Mn accumulates via a Pho84p phosphate transporter; (iii) SPCA1 and SPCA2 sequester and eliminate the excess Mn in vacuoles that are expelled from the cell.

4.4. *In vivo* biodistribution of Mn_xO_y NPs

Multiple Mn_xO_y NPs with different morphologies have been evaluated for cancer therapy. However, these structures are intertwined with other relevant co-adjutant players such polymers, metals or organic molecules (see Fig. 2 and Tables 1 and 2). This heterogeneity burdens a systematic analysis to explore the specific influence of morphology in the biodistribution. In the case of 100 nm sized- MnO_2 nanosheets, Tang et al. [43] reported a predominant accumulation in the liver (12.48% ID/g) followed by the kidneys (5.14%ID/g) and spleen (4.75% ID/g) after 48 h of intravenous injection. Analogous pathways were found for Mn-decorated nanoplateforms regardless of whether Mn was either in form of MnO_2 [69] or inserted in a bimetallic spinel ($MnFe_2O_4$). Feng et al. [69] found a%ID/g for liver, kidney and spleen of 18.30, 12.48 and 17.50%, respectively after 48 h of the intravenous injection of 24 nm MnO_2 - Fe_5C_2 . Biodistribution analysis of 6 nm $MnFe_2O_4$ nanocrystals supported onto 50 nm-sized mesoporous silica NPs also revealed a preferential accumulation in the liver [76]. In these works [43,69,76], the authors suggested a preferential excretion through reticuloendothelial system (i.e. macrophage phagocytosis and) which in fact is in agreement with other NPs of analogous sizes [150]. Similar results were also reported for 20-nm MnO particles embedded within organic vesicles [151]. It is also noteworthy that a functionalization of Mn-decorated nanoplateforms with PEG increase the blood circulation and hence, the tumor EPR effect leading to a larger accumulation in tumor tissue in comparison to other organs as liver, kidney or spleen [152]. Given the heterogeneity of the studied systems, (i.e. Mn is combined with different elements) it is difficult to establish clear patterns for an optimal morphology able to reach the tumor site. The most efficient strategy seems to cloak the Mn-containing nanostructures with cell membranes [72,124] reaching good tumor targeting even with 200 nm sized MOF NPs coated with MnO_2 . The main advantage of the use of cell membranes is not only to extend the blood half-life to increase the uptake within the tumor, but also increase the selectivity towards cancer cells via an active targeting [153,154].

5. Oxidase mimicking activity of Mn_xO_y NPs for cancer starvation therapy

O_2 -generation, GSH-depletion and $\bullet OH$ production activities of Mn_xO_y have been the most explored options so far as enzyme-like mimicking candidates for biomedical applications. However, some catalytic nanomaterials may also transform the dissolved O_2 into ROS [155] or oxidize key biomolecules such as glucose [156], which in fact are reactions to exploit in cancer therapy. Recent studies also suggest that MnO_2 nanosheets (NSs) may hold a promising future as oxidase surrogates for potential application in cancer therapy. As previously mentioned, the so-called ‘‘Warburg Effect’’ describes the enhanced glucose consumption detected in tumor cells that operate under hypoxic conditions with highly inefficient metabolism [157]. Under rapid cell proliferation conditions, energy obtaining occurs in cancer cells preferentially through glucose fermentation into lactic acid instead of a complete oxidation via the tricarboxylic acid (TCA) cycle followed by oxidative phosphorylation [158]. As a result, this energy production through a high rate of glycolysis followed by lactic acid fermentation, allows different advantages. This alternative permits a higher production of additional metabolites that can be used by cells along proliferation (ribose sugars needed for nucleotides, glycerol and citrate for lipids and nonessential amino acids).

Although it is less efficient than oxidative phosphorylation in terms of ATP generation, the conversion of glucose into abundant ATP is still possible. Under these conditions, the glycolytic flux compensates the low yield of ATP per glucose consumed. Thus, cellular ATP obtained via glycolysis exceeds that produced from oxidative phosphorylation. Consequently, Warburg effect benefits both bioenergetics and biosynthesis within cell [158]. Besides glucose, an alternative source of

anaplerosis (i.e. reaction which supply cell with Krebs cycle-intermediates) in cells occurs through metabolism of amino acids, particularly glutamine. Cells can partially oxidize glutamine in an analogous way to partial oxidation of glucose along aerobic glycolysis. Since glutaminolysis uses several steps of the TCA cycle, redirecting glucose and glutamine into anabolic pathways, those results in a very efficient strategy for cancer cell in order to survive [8, 158,159]. Thus, trying to deprive cancer cells of glucose and amino acids can result in depletion of TCA cycle intermediates. This means that both energy obtaining and biosynthesis are altered in cells (i.e. de novo production of nucleotides depends on glutamine as a nitrogen source and glucose as a carbon one) [158]. Then starvation therapy tries to deprive relevant metabolites in order to control tumor growth acting simultaneously through different pathways. Simultaneously, MnO_2 NSs have recently shown promising results as GOx mimicking candidates to deplete glucose from cancer cells to alter their metabolism and restrict their growth, as illustrated Fig. 7a.

Lis group first reported [41] glucose-oxidase like activity for MnO_2 NSs under a wide pH range, presenting Michaelis-Menten constant (K_M) values of 21 mM that in comparison with natural GOx K_M (34 mM) [160] shows more affinity towards glucose. Furthermore, Tang et al. [43] fabricated 2D MnO_2 ultrathin NSs via BSA-assisted wet-chemical method. The classic synthesis of MnO_2 nanostructures from Mn^{2+} and $NaOH/O_2$ system was modified adding BSA in order to form a novel 2D structure and enhance the stability in biological medium while preventing further agglomeration or Mn^{2+} leaching. Interestingly, MnO_2 NSs exhibited glucose-oxidase activity, with an apparent K_M of 26.4 mM. This apparently stronger affinity towards glucose and its intrinsic GOx-like activity was evaluated in cancer starvation-therapy. These nanosheets led to an 80% decrease in cellular ATP (adenosine triphosphate) levels, the main product of glucose metabolism, after 12 h. Subsequent *in vivo* studies confirmed the therapeutic efficiency of MnO_2 NSs. This case represents one of the first examples of glucose-oxidase mimetic activity in Mn related materials and paves the way to the specific influence of NP shape to promote one type of enzyme-mimicking response in detriment of others.

Chen's group also took advantage of the simultaneous catalytic response of MnO_2 NSs [42] towards glucose, and the previously mentioned reactivity with H_2O_2 and GSH, thereby resulting in a quite interesting and efficient synergy between the generation of O_2 and their consumption (GOx-like activity), represented in Fig. 7a. Moreover, the interaction of MnO_2 NSs with rich GSH environments yield Mn^{2+} production that can activate ROS production as it was discussed in the previous section (Fig. 5b). The global process results in an efficient and selective death of tumor cells. MnO_2 oxidase mechanism was approached by Meng et al. by studying the effect of the crystal structure and surface chemistry on TMB (3,3',5,5'-Tetramethylbenzidine) oxidation [161]. The increase of OH^- groups onto the surface of MnO_2 promoted a major availability of active catalytic sites that ended up favoring the oxidation reaction [162] (see Fig. 7b(i)). In addition, these hydroxyl groups increased the affinity towards TMB substrates in accordance with the lower K_M reported. Remarkably, a fraction of Mn^{4+} was also essential to ensure a regeneration of OH^- groups (Fig. 7b (i) and (ii)). EPR experiments highlighted the generation of ROS species ($\bullet O_2^-$, $\bullet OH$ and 1O_2) which also contributed to their oxidative capability. Specifically, the oxidase activity followed the trend: β - $MnO_2 > \alpha$ - $MnO_2 > \gamma$ - MnO_2 based on the optimal OH^-/Mn^{4+} ratio. A similar trend was found by Hayashi et al. [163] in the oxidation of 5-hydroxymethylfurfural.

In general terms, crystalline structure and catalytic activity are typically related in heterogeneous catalysis. Although in several catalytic contexts (i.e. Volatile organic compounds catalytic oxidation or electrocatalysis) the effect of crystalline structure is deeply investigated, in terms of cancer therapy no conclusive correlation between catalytic activity and crystalline structure has been established so far, even though multiple Mn_xO_y structures (i.e., λ - MnO_2 [74], α - MnO_2 [164] or

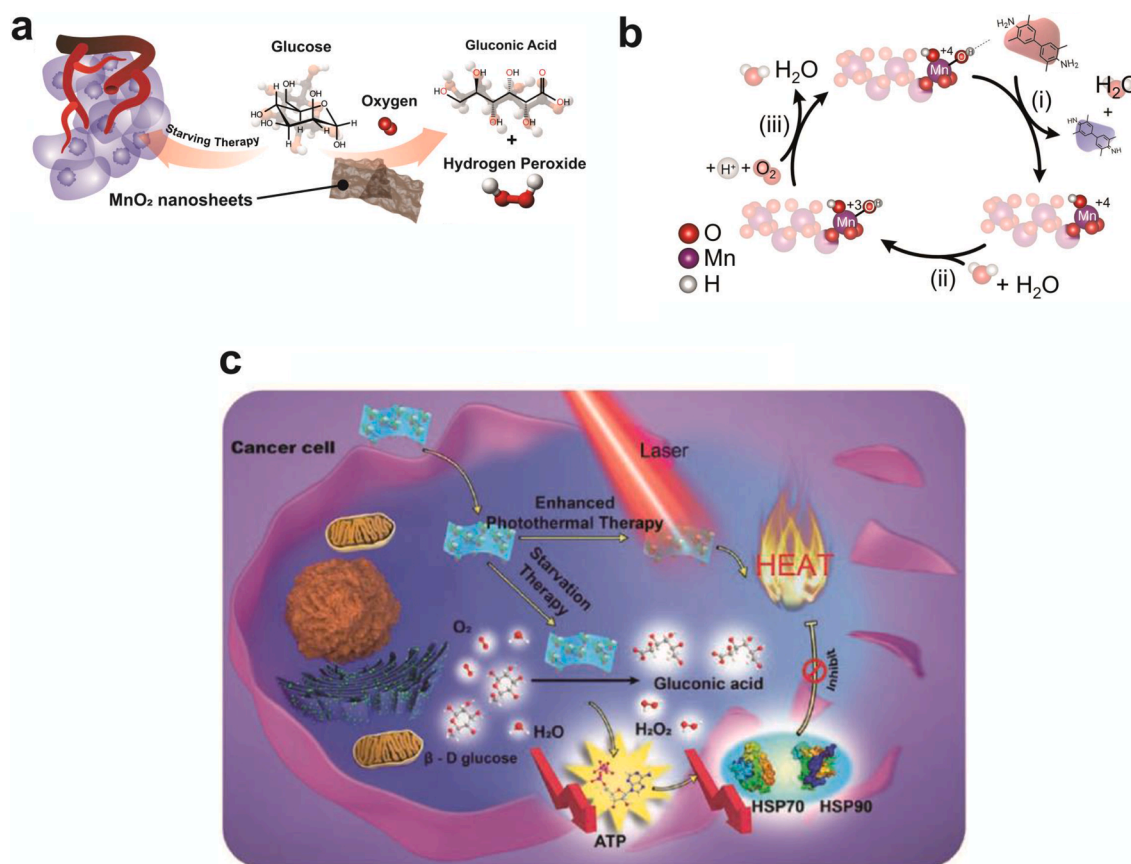


Fig. 7. (a) Schematic illustration comprising larger glucose consumption by tumor cells (Warburg effect) and mechanism of action of MnO₂ nanosheets. The catalytic conversion of glucose into gluconic acid and H₂O₂ avoids their entrance into diverse metabolic pathways like mitochondrial respiration (specifically, this will block main ATP production route), resulting in a disrupted metabolic process; (b) MnO₂-catalyzed TMB oxidation mechanism. In a first step (i) TMB reacts with OH⁻ groups on MnO₂ surface; (ii) To regenerate the active OH⁻ groups, Mn⁴⁺ can be reduced by H₂O molecules to Mn³⁺; (iii) Finally, molecular O₂ can re-oxidize reduced Mn to regenerate the active species [161]; (c) Therapeutic application of GOx-like MnO₂ nanosheets, and the implications regarding the decrease in ATP, HSP70 and HSP90. Reproduced with permission from [43] Copyright 2018, Wiley-VCH.

Birnessite [129] have been identified [40]. In this regard, more exhaustive and systematic studies are still necessary to determine the role of the crystalline structure to take a step forward the design of the ideal nanopatform.

6. Conclusions and outlook

Several studies endorse the Mn-based nanomaterials with a high potential as therapeutic agents in the TME. By taking advantage of their reactivity and catalytic response, it is possible to overcome the detrimental TME conditions and locally increase O₂ concentration, decrease the amount of antioxidants such as GSH and/or nutrients (i.e. mimicking the GOx activity). Mn_xO_y NPs do not only show high intrinsic activity but also positive synergistic effects in combination with different Mn_xO_y could efficiently supply them with O₂ by using endogenously generated tumor intracellular H₂O₂. Alternative, Mn-based nanosystems may also significantly increase ROS levels with the aid of PSs or reducing the availability of GSH. All these facts make Mn_xO_y a promising candidate to boost the efficacies of new nanocatalytic medicine therapies.

However, Mn_xO_y NPs still face several challenges. In terms of chemical reactivity, a deeper understanding in the mechanisms and substrate selectivity remains unclear and further studying is still necessary. The activity of inorganic Mn-based nanocatalysts in heterogeneous catalysis depends on multiple physicochemical factors: size, shape, surface properties (like charge, composition or ligands), crystalline order or stability (pH, temperature). Such variability not only hinders a deep understanding of the catalysis, but also the reliable

comparison of gathered results in the literature. Regarding biosafety, larger Mn_xO_y NPs may be less prone to be properly excreted [35] and accumulate in certain organs. Long-term exposures may also induce damage in the nerve system. Although Mn_xO_y NPs possess good biocompatibility and low toxicity at certain levels, most of current studies focus on Mn_xO_y theranostic performance rather than establishing clear cytotoxicity patterns. Still, no Mn_xO_y NPs have been translated into clinical phase. Taking into account the mentioned bottlenecks, rigorous and systematic bio-safety *in vivo* evaluations are still necessary to pave the way towards the same clinical status as other inorganic nano-formulations for cancer therapy [165]. Furthermore, a complete understanding of the interplay and balance between homogeneous and heterogeneous mechanisms must be pursued. Nevertheless, considering the discussed TME characteristics and how the chemical reactivity of Mn_xO_y fit in, they are certainly strong candidates for the near future implementation of Nanocatalytic medicine towards cancer therapy. Devising smart biomimetic cloaking systems and combining new configurations based on planar configurations, low-ordered crystalline structures or even single atom formulations show promising results for the Mn-based material design. Still, the combination with co-adjuvants active players or with promising strategies like immunotherapy will be required to develop full and effective treatments able to translate into clinical.

Declaration of Competing Interest

The authors declare that they have no known competing financial

interests or personal relationships that could have appeared to influence the work reported in this paper.

Data availability

No data was used for the research described in the article.

Acknowledgments

Financial support from the European Research Council (ERC Advanced Grant CADENCE number 742684) is gratefully acknowledged. J.B.-A. thanks the Spanish Government for an FPU predoctoral contract.

References

- [1] J. Ferlay, E. Steliarova-Foucher, J. Lortet-Tieulent, S. Rosso, J.W.W. Coebergh, H. Comber, D. Forman, F. Bray, Cancer incidence and mortality patterns in Europe: estimates for 40 countries in 2012, *Eur. J. Cancer* 49 (2013) 1374–1403.
- [2] S. Tohme, R.L. Simmons, A. Tsung, Surgery for cancer: a trigger for metastases, *Cancer Res.* 77 (2017) 1548–1552.
- [3] Z. Li, S. Tan, S. Li, Q. Shen, K. Wang, Cancer drug delivery in the nano era: an overview and perspectives (Review), *Oncol. Rep.* 38 (2017) 611–624.
- [4] Y. Li, K.H. Yun, H. Lee, S.H. Goh, Y.G. Suh, Y. Choi, Porous platinum nanoparticles as a high-Z and oxygen generating nanozyme for enhanced radiotherapy *in vivo*, *Biomaterials* 197 (2019) 12–19.
- [5] S. Yang, H. Gao, Nanoparticles for modulating tumor microenvironment to improve drug delivery and tumor therapy, *Pharmacol. Res.* 126 (2017) 97–108.
- [6] Y. Dai, C. Xu, X. Sun, X. Chen, Nanoparticle design strategies for enhanced anticancer therapy by exploiting the tumour microenvironment, *Chem. Soc. Rev.* 46 (2017) 3830–3852.
- [7] T. Wu, Y. Dai, Tumor microenvironment and therapeutic response, *Cancer Lett.* 387 (2017) 61–68.
- [8] M.G. Vander Heiden, L.C. Cantley, C.B. Thompson, Understanding the warburg effect: the metabolic requirements of cell proliferation, *Science* 324 (2009) 1029.
- [9] F. Hillen, A.W. Griffioen, Tumour vascularization: sprouting angiogenesis and beyond, *Cancer Metastasis Rev.* 26 (2007) 489–502.
- [10] K. Greish, Enhanced Permeability and Retention (EPR) effect for anticancer nanomedicine drug targeting, in: S.R. Grobmyer, B.M. Moudgil (Eds.), *Cancer Nanotechnology: Methods and Protocols*, Humana Press, Totowa, NJ, 2010, pp. 25–37.
- [11] V. Sosa, T. Moliné, R. Somoza, R. Paciucci, H. Kondoh, M.E. Lleonart, Oxidative stress and cancer: an overview, *Ageing Res. Rev.* 12 (2013) 376–390.
- [12] M. López-Lázaro, Dual role of hydrogen peroxide in cancer: possible relevance to cancer chemoprevention and therapy, *Cancer Lett.* 252 (2007) 1–8.
- [13] H. Pelicano, D. Carney, P. Huang, ROS stress in cancer cells and therapeutic implications, *Drug Resist. Updat.* 7 (2004) 97–110.
- [14] M. Zieba, M. Suwalski, S. Kwiatkowska, G. Piasecka, I. Grzelewska-Rzymowska, R. Stolarek, D. Nowak, Comparison of hydrogen peroxide generation and the content of lipid peroxidation products in lung cancer tissue and pulmonary parenchyma, *Respir. Med.* 94 (2000) 800–805.
- [15] R.H. Burdon, Superoxide and hydrogen peroxide in relation to mammalian cell proliferation, *Free Radical Biol. Med.* 18 (1995) 775–794.
- [16] X. Zhang, Y. Lin, R.J. Gillies, Tumor pH and its measurement, *J. Nucl. Med.* 51 (2010) 1167–1170.
- [17] P. Kuppusamy, H. Li, G. Ilangoan, A.J. Cardounel, J.L. Zweier, K. Yamada, M. C. Krishna, J.B. Mitchell, Noninvasive imaging of tumor redox status and its modification by tissue glutathione levels, *Cancer Res.* 62 (2002) 307.
- [18] R. Franco, J.A. Cidlowski, Apoptosis and glutathione: beyond an antioxidant, *Cell Death Differ.* 16 (2009) 1303–1314.
- [19] J. Bonet-Aleta, M. Sancho-Albero, J. Calzada-Funes, S. Irusta, P. Martin-Duque, J. L. Hueso, J. Santamaria, Glutathione-triggered catalytic response of copper-iron mixed oxide nanoparticles. Leveraging tumor microenvironment conditions for chemodynamic therapy, *J. Colloid Interface Sci.* 617 (2022) 704–717.
- [20] G.Y. Liou, P. Storz, Reactive oxygen species in cancer, *Free Radic. Res.* 44 (2010) 479–496.
- [21] Y. Guo, Y. Xu, Q. Bao, C. Shen, D. Ni, P. Hu, J. Shi, Endogenous copper for nanocatalytic oxidative damage and self-protection pathway breakage of cancer, *ACS Nano* 15 (2021) 16286–16297.
- [22] O. Trédan, C.M. Galmarini, K. Patel, I.F. Tannock, Drug resistance and the solid tumor microenvironment, *J. Natl. Cancer Inst.* 99 (2007) 1441–1454.
- [23] S. Gai, G. Yang, P. Yang, F. He, J. Lin, D. Jin, B. Xing, Recent advances in functional nanomaterials for light-triggered cancer therapy, *Nano Today* 19 (2018) 146–187.
- [24] B. Ding, P. Zheng, P.a. Ma, J. Lin, Manganese oxide nanomaterials: synthesis, properties, and theranostic applications, *Adv. Mater.* 32 (2020), 1905823.
- [25] Y. Ding, Y. Dai, M. Wu, L. Li, Glutathione-mediated nanomedicines for cancer diagnosis and therapy, *Chem. Eng. J.* 426 (2021), 128880.
- [26] S. Yu, Z. Chen, X. Zeng, X. Chen, Z. Gu, Advances in nanomedicine for cancer starvation therapy, *Theranostics* 9 (2019) 8026–8047.
- [27] L.H. Fu, C. Qi, J. Lin, P. Huang, Catalytic chemistry of glucose oxidase in cancer diagnosis and treatment, *Chem. Soc. Rev.* 47 (2018) 6454–6472.
- [28] H. Wang, L. Cheng, S. Ma, L. Ding, W. Zhang, Z. Xu, D. Li, L. Gao, Self-assembled multiple enzyme composites for enhanced synergistic cancer starving-catalytic therapy, *ACS Appl. Mater. Interfaces* 12 (2020) 20191–20201.
- [29] H. Wei, E. Wang, Nanomaterials with enzyme-like characteristics (nanozymes): next-generation artificial enzymes, *Chem. Soc. Rev.* 42 (2013) 6060–6093.
- [30] X. Wang, Y. Hu, H. Wei, Nanozymes in bionanotechnology: from sensing to therapeutics and beyond, *Inorg. Chem. Front.* 3 (2016) 41–60.
- [31] J. Wu, X. Wang, Q. Wang, Z. Lou, S. Li, Y. Zhu, L. Qin, H. Wei, Nanomaterials with enzyme-like characteristics (nanozymes): next-generation artificial enzymes (II), *Chem. Soc. Rev.* 48 (2019) 1004–1076.
- [32] H. Kobayashi, A. Fukuoka, Synthesis and utilisation of sugar compounds derived from lignocellulosic biomass, *Green Chem.* 15 (2013) 1740–1763.
- [33] Y. Ding, H. Xu, C. Xu, Z. Tong, S. Zhang, Y. Bai, Y. Chen, Q. Xu, L. Zhou, H. Ding, Z. Sun, S. Yan, Z. Mao, W. Wang, A nanomedicine fabricated from gold nanoparticles-decorated metal-organic framework for cascade chemo/chemodynamic cancer therapy, 7 (2020) 2001060.
- [34] Z. Zhang, Y. Ji, Nanostructured manganese dioxide for anticancer applications: preparation, diagnosis, and therapy, *Nanoscale* 12 (2020) 17982–18003.
- [35] D. Nie, Y. Zhu, T. Guo, M. Yue, M. Lin, Research advance in manganese nanoparticles in cancer diagnosis and therapy, *Front. Mater.* 9 (2022), 857385.
- [36] C. Jiang, T. He, Q. Tang, J. He, Q. Ren, D.Y. Zhang, B. Gurrum, N.T. Blum, Y. Chen, P. Huang, J. Lin, Nanozyme catalyzed cascade reaction for enhanced chemodynamic therapy of low-H₂O₂ tumor, *Appl. Mater. Today* 26 (2022), 101357.
- [37] Y. Zhu, W. Wang, J. Cheng, Y. Qu, Y. Dai, M. Liu, J. Yu, C. Wang, H. Wang, S. Wang, C. Zhao, Y. Wu, Y. Liu, Stimuli-responsive manganese single-atom nanozyme for tumor therapy via integrated cascade reactions, *Angew. Chem. Int. Ed.* 60 (2021) 9480–9488.
- [38] Y.F. Chang, J.G. McCarty, Novel oxygen storage components for advanced catalysts for emission control in natural gas fueled vehicles, *Catal. Today* 30 (1996) 163–170.
- [39] H. Huang, Y. Xu, Q. Feng, D.Y.C. Leung, Low temperature catalytic oxidation of volatile organic compounds: a review, *Catal. Sci. Technol.* 5 (2015) 2649–2669.
- [40] S.K. Ghosh, Diversity in the family of manganese oxides at the nanoscale: from fundamentals to applications, *ACS Omega* 5 (2020) 25493–25504.
- [41] L. Han, H. Zhang, D. Chen, F. Li, Protein-directed metal oxide nanoflakes with tandem enzyme-like characteristics: colorimetric glucose sensing based on one-pot enzyme-free cascade catalysis, *Adv. Funct. Mater.* 28 (2018), 1800018.
- [42] N. Yan, L. Lin, C. Xu, H. Tian, X. Chen, A GSH-gated DNA nanodevice for tumor-specific signal amplification of microRNA and MR imaging-guided theranostics, *Small* 15 (2019), 1903016.
- [43] W. Tang, W. Fan, W. Zhang, Z. Yang, L. Li, Z. Wang, Y.L. Chiang, Y. Liu, L. Deng, L. He, Z. Shen, O. Jacobson, M.A. Aronova, A. Jin, J. Xie, X. Chen, Wet/Sonochemical synthesis of enzymatic two-dimensional MnO₂ nanosheets for synergistic catalysis-enhanced phototheranostics, *Adv. Mater.* 31 (2019), 1900401.
- [44] E. Ember, S. Rothbart, R. Puchta, R. van Eldik, Metal ion-catalyzed oxidative degradation of Orange II by H₂O₂. High catalytic activity of simple manganese salts, *New J. Chem.* 33 (2009) 34–49.
- [45] L.Z. Gao, J. Zhuang, L. Nie, J.B. Zhang, Y. Zhang, N. Gu, T.H. Wang, J. Feng, D. L. Yang, S. Perrett, X. Yan, Intrinsic peroxidase-like activity of ferromagnetic nanoparticles, *Nat. Nanotechnol.* 2 (2007) 577–583.
- [46] F. Gao, Y. Tang, W.L. Liu, M.Z. Zou, C. Huang, C.J. Liu, X.Z. Zhang, Intra/extracellular lactic acid exhaustion for synergistic metabolic therapy and immunotherapy of tumors, *Adv. Mater.* 31 (2019), 1904639.
- [47] M. Lv, M. Chen, R. Zhang, W. Zhang, C. Wang, Y. Zhang, X. Wei, Y. Guan, J. Liu, K. Feng, M. Jing, X. Wang, Y.C. Liu, Q. Mei, W. Han, Z. Jiang, Manganese is critical for antitumor immune responses via cGAS-STING and improves the efficacy of clinical immunotherapy, *Cell Res.* 30 (2020) 966–979.
- [48] G. Yang, L. Xu, J. Xu, R. Zhang, G. Song, Y. Chao, L. Feng, F. Han, Z. Dong, B. Li, Z. Liu, Smart nanoreactors for pH-responsive tumor homing, mitochondria-targeting, and enhanced photodynamic-immunotherapy of cancer, *Nano Lett.* 18 (2018) 2475–2484.
- [49] M. Pourbaix, *Atlas of electrochemical equilibria in aqueous solutions*, (1974).
- [50] Z. Liu, S. Zhang, H. Lin, M. Zhao, H. Yao, L. Zhang, W. Peng, Y. Chen, Theranostic 2D ultrathin MnO₂ nanosheets with fast responsibility to endogenous tumor microenvironment and exogenous NIR irradiation, *Biomaterials* 155 (2018) 54–63.
- [51] L. Yu, Y. Chen, M. Wu, X. Cai, H. Yao, L. Zhang, H. Chen, J. Shi, Manganese extraction" strategy enables tumor-sensitive biodegradability and theranostics of nanoparticles, *J. Am. Chem. Soc.* 138 (2016) 9881–9894.
- [52] L.S. Lin, J. Song, L. Song, K. Ke, Y. Liu, Z. Zhou, Z. Shen, J. Li, Z. Yang, W. Tang, G. Niu, H.H. Yang, X. Chen, Simultaneous fenton-like ion delivery and glutathione depletion by MnO₂-based nanoagent to enhance chemodynamic therapy, *Angew. Chem. Int. Ed.* 57 (2018) 4902–4906.
- [53] R. Liang, L. Liu, H. He, Z. Chen, Z. Han, Z. Luo, Z. Wu, M. Zheng, Y. Ma, L. Cai, Oxygen-boosted immunogenic photodynamic therapy with gold nanocages@ manganese dioxide to inhibit tumor growth and metastases, *Biomaterials* 177 (2018) 149–160.
- [54] R. Wei, X. Gong, H. Lin, K. Zhang, A. Li, K. Liu, H. Shan, X. Chen, J. Gao, Versatile octapod-shaped hollow porous manganese(II) oxide nanoplateform for real-time visualization of cargo delivery, *Nano Lett.* 19 (2019) 5394–5402.

- [55] S. Ren, J. Yang, L. Ma, X. Li, W. Wu, C. Liu, J. He, L. Miao, Ternary-responsive drug delivery with activatable dual mode contrast-enhanced *in vivo* imaging, *ACS Appl. Mater. Interfaces* 10 (2018) 31947–31958.
- [56] T.L. Moore, L. Rodriguez-Lorenzo, V. Hirsch, S. Balog, D. Urban, C. Jud, B. Rothen-Rutishauser, M. Lattuada, A. Petri-Fink, Nanoparticle colloidal stability in cell culture media and impact on cellular interactions, *Chem. Soc. Rev.* 44 (2015) 6287–6305.
- [57] Y. Cao, X. Meng, D. Wang, K. Zhang, W. Dai, H. Dong, X. Zhang, Intelligent MnO₂/Cu₂-xS for multimode imaging diagnostic and advanced single-laser irradiated photothermal/photodynamic therapy, *ACS Appl. Mater. Interfaces* 10 (2018) 17732–17741.
- [58] J. Liu, Q. Chen, W. Zhu, X. Yi, Y. Yang, Z. Dong, Z. Liu, Nanoscale-coordination-polymer-shelled manganese dioxide composite nanoparticles: a multistage redox/pH/H₂O₂-responsive cancer theranostic nanoplatfom, *Adv. Funct. Mater.* 27 (2017), 1605926.
- [59] C. Zhang, W.H. Chen, L.H. Liu, W.X. Qiu, W.Y. Yu, X.Z. Zhang, An O₂ self-supplementing and reactive-oxygen-species-circulating amplified nanoplatfom via H₂O/H₂O₂ splitting for tumor imaging and photodynamic therapy, *Adv. Funct. Mater.* 27 (2017), 1700626.
- [60] B. Ding, S. Shao, F. Jiang, P. Dang, C. Sun, S. Huang, P.A. Ma, D. Jin, A.A. A. Kheraif, J. Lin, MnO₂-disguised upconversion hybrid nanocomposite: an ideal architecture for tumor microenvironment-triggered UCL/MR bioimaging and enhanced chemodynamic therapy, *Chem. Mater.* 31 (2019) 2651–2660.
- [61] D. Gu, P. An, X. He, H. Wu, Z. Gao, Y. Li, F. Chen, K. Cheng, Y. Zhang, C. You, B. Sun, A novel versatile yolk-shell nanosystem based on NIR-elevated drug release and GSH depletion-enhanced Fenton-like reaction for synergistic cancer therapy, *Colloids Surf. B* 189 (2020), 110810.
- [62] X. Yi, L. Chen, X. Zhong, R. Gao, Y. Qian, F. Wu, G. Song, Z. Chai, Z. Liu, K. Yang, Core-shell Au@MnO₂ nanoparticles for enhanced radiotherapy via improving the tumor oxygenation, *Nano Res.* 9 (2016) 3267–3278.
- [63] W. Zhu, Z. Dong, T. Fu, J. Liu, Q. Chen, Y. Li, R. Zhu, L. Xu, Z. Liu, Modulation of hypoxia in solid tumor microenvironment with MnO₂ nanoparticles to enhance photodynamic therapy, *Adv. Funct. Mater.* 26 (2016) 5490–5498.
- [64] G. Yang, L. Xu, Y. Chao, J. Xu, X. Sun, Y. Wu, R. Peng, Z. Liu, Hollow MnO₂ as a tumor-microenvironment-responsive biodegradable nano-platfom for combination therapy favoring antitumor immune responses, *Nat. Commun.* 8 (2017) 902.
- [65] G. Yang, R. Zhang, C. Liang, H. Zhao, X. Yi, S. Shen, K. Yang, L. Cheng, Z. Liu, Manganese dioxide coated WS₂@Fe₃O₄/sSiO₂ nanocomposites for pH-responsive MR imaging and oxygen-elevated synergistic therapy, *Small* 14 (2018), 1702664.
- [66] Y. Zhang, Y. Cao, T. Gao, Y. Kuang, Z. An, Z. Mao, Y. He, J. Yan, Z. Lu, R. Pei, Tumor microenvironment-responsive and catalytic cascade-enhanced nanocomposite for tumor thermal ablation synergizing with chemodynamic and chemotherapy, *ACS Appl. Bio Mater.* 3 (2020) 3880–3893.
- [67] Y.H. Zhang, W.X. Qiu, M. Zhang, L. Zhang, X.Z. Zhang, MnO₂ motor: a prospective cancer-starving therapy promoter, *ACS Appl. Mater. Interfaces* 10 (2018) 15030–15039.
- [68] P. Prasad, C.R. Gordijo, A.Z. Abbasi, A. Maeda, A. Ip, A.M. Rauth, R.S. DaCosta, X. Y. Wu, Multifunctional albumin-MnO₂ nanoparticles modulate solid tumor microenvironment by attenuating hypoxia, acidosis, vascular endothelial growth factor and enhance radiation response, *ACS Nano* 8 (2014) 3202–3212.
- [69] L. Feng, R. Xie, C. Wang, S. Gai, F. He, D. Yang, P. Yang, J. Lin, Magnetic targeting, tumor microenvironment-responsive intelligent nanocatalysts for enhanced tumor ablation, *ACS Nano* 12 (2018) 11000–11012.
- [70] M. Yu, X. Duan, Y. Cai, F. Zhang, S. Jiang, S. Han, J. Shen, X. Shuai, Multifunctional nanoregulator reshapes immune microenvironment and enhances immune memory for tumor immunotherapy, *Adv. Sci.* 6 (2019), 1900037.
- [71] D. Zhu, M. Lyu, W. Jiang, M. Suo, Q. Huang, K. Li, Biomimetic nanozymes/camptothecin hybrid system for synergistically enhanced radiotherapy, *J. Mater. Chem. B* 8 (2020) 5312–5319.
- [72] X. Yang, Y. Yang, F. Gao, J.J. Wei, C.G. Qian, M.J. Sun, Biomimetic hybrid nanozymes with self-supplied H⁺ and accelerated O₂ generation for enhanced starvation and photodynamic therapy against hypoxic tumors, *Nano Lett.* 19 (2019) 4334–4342.
- [73] L. Jiao, H.Y. Yan, Y. Wu, W.L. Gu, C.Z. Zhu, D. Du, Y.H. Lin, When nanozymes meet single-atom catalysis, *Angew. Chem. Int. Ed.* 59 (2020) 2565–2576.
- [74] T. He, H. Xu, Y. Zhang, S. Yi, R. Cui, S. Xing, C. Wei, J. Lin, P. Huang, Glucose oxidase-instructed traceable self-oxygenation/hyperthermia dually enhanced cancer starvation therapy, *Theranostics* 10 (2020) 1544–1554.
- [75] X. Jing, Y. Xu, D. Liu, Y. Wu, N. Zhou, D. Wang, K. Yan, L. Meng, Intelligent nanoflowers: a full tumor microenvironment-responsive multimodal cancer theranostic nanoplatfom, *Nanoscale* 11 (2019) 15508–15518.
- [76] J. Kim, H.R. Cho, H. Jeon, D. Kim, C. Song, N. Lee, S.H. Choi, T. Hyeon, Continuous O₂-evolving MnFe₂O₄ nanoparticle-anchored mesoporous silica nanoparticles for efficient photodynamic therapy in hypoxic cancer, *J. Am. Chem. Soc.* 139 (2017) 10992–10995.
- [77] Z. Ma, X. Jia, J. Bai, Y. Ruan, C. Wang, J. Li, M. Zhang, X. Jiang, MnO₂ gatekeeper: an intelligent and O₂-evolving shell for preventing premature release of high cargo payload core, overcoming tumor hypoxia, and acidic H₂O₂-sensitive MRI, *Adv. Funct. Mater.* 27 (2017), 1604258.
- [78] Y. Yao, N. Li, X. Zhang, J. Ong'achwa Machuki, D. Yang, Y. Yu, J. Li, D. Tang, J. Tian, F. Gao, DNA-templated silver nanocluster/porphyrin/MnO₂ platform for label-free intracellular Zn²⁺ imaging and fluorescence-/magnetic resonance imaging-guided photodynamic therapy, *ACS Appl. Mater. Interfaces* 11 (2019) 13991–14003.
- [79] P. Zhu, Y. Chen, J. Shi, Nanoenzyme-augmented cancer sonodynamic therapy by catalytic tumor oxygenation, *ACS Nano* 12 (2018) 3780–3795.
- [80] J. Liu, P. Du, T. Liu, B.J. Córdoba Wong, W. Wang, H. Ju, J. Lei, A black phosphorus/manganese dioxide nanoplatfom: oxygen self-supply monitoring, photodynamic therapy enhancement and feedback, *Biomaterials* 192 (2019) 179–188.
- [81] I. Fita, M.G. Rossmann, The active center of catalase, *J. Mol. Biol.* 185 (1985) 21–37.
- [82] M.C. Denler, G.B. Wijeratne, D.B. Rice, H.E. Colmer, V.W. Day, T.A. Jackson, MnIII-Peroxo adduct supported by a new tetradentate ligand shows acid-sensitive aldehyde deformylation reactivity, *Dalton Trans.* 47 (2018) 13442–13458.
- [83] J. Reedijk, E. Bouwman, *Bioinorganic Catalysis*, CRC Press, 1999.
- [84] F.A. Armstrong, Why did nature choose manganese to make oxygen? *Philos. Trans. R. Soc. B Biol. Sci.* 363 (2008) 1263–1270.
- [85] Q. Chen, L. Feng, J. Liu, W. Zhu, Z. Dong, Y. Wu, Z. Liu, Intelligent albumin-MnO₂ nanoparticles as pH-/H₂O₂-responsive dissociable nanocarriers to modulate tumor hypoxia for effective combination therapy, *Adv. Mater.* 28 (2016) 7129–7136.
- [86] W. Fan, W. Bu, B. Shen, Q. He, Z. Cui, Y. Liu, X. Zheng, K. Zhao, J. Shi, Intelligent MnO₂ nanosheets anchored with upconversion nanoprobles for concurrent pH-/H₂O₂-responsive UCL imaging and oxygen-elevated synergistic therapy, *Adv. Mater.* 27 (2015) 4155–4161.
- [87] S.H. Do, B. Batchelor, H.K. Lee, S.H. Kong, Hydrogen peroxide decomposition on manganese oxide (pyrolusite): kinetics, intermediates, and mechanism, *Chemosphere* 75 (2009) 8–12.
- [88] W. Zhang, S. Li, X. Liu, C. Yang, N. Hu, L. Dou, B. Zhao, Q. Zhang, Y. Suo, J. Wang, Oxygen-generating MnO₂ nanodots-anchored versatile nanoplatfom for combined chemo-photodynamic therapy in hypoxic cancer, *Adv. Funct. Mater.* 28 (2018), 1706375.
- [89] Q. Tang, Z. Cheng, N. Yang, Q. Li, P. Wang, D. Chen, W. Wang, X. Song, X. Dong, Hydrangea-structured tumor microenvironment responsive degradable nanoplatfom for hypoxic tumor multimodal imaging and therapy, *Biomaterials* 205 (2019) 1–10.
- [90] S. Zhang, Q. Li, N. Yang, Y. Shi, W. Ge, W. Wang, W. Huang, X. Song, X. Dong, Phase-change materials based nanoparticles for controlled hypoxia modulation and enhanced phototherapy, *Adv. Funct. Mater.* 29 (2019), 1906805.
- [91] N. Singh, M. Geethika, S.M. Eswarappa, G. Muges, Manganese-based nanozymes: multienzyme redox activity and effect on the nitric oxide produced by endothelial nitric oxide synthase, *Chem. A Eur. J.* 24 (2018) 8393–8403.
- [92] N. Singh, M.A. Savanur, S. Srivastava, P. D'Silva, G. Muges, A redox modulatory Mn₃O₄ nanozyme with multi-enzyme activity provides efficient cytoprotection to human cells in a Parkinson's disease model, *Angew. Chem. Int. Ed.* 56 (2017) 14267–14271.
- [93] X.L. Luo, J.J. Xu, W. Zhao, H.Y. Chen, A novel glucose ENFET based on the special reactivity of MnO₂ nanoparticles, *Biosens. Bioelectron.* 19 (2004) 1295–1300.
- [94] S. Gao, G. Wang, Z. Qin, X. Wang, G. Zhao, Q. Ma, L. Zhu, Oxygen-generating hybrid nanoparticles to enhance fluorescent/photoacoustic/ultrasound imaging guided tumor photodynamic therapy, *Biomaterials* 112 (2017) 324–335.
- [95] A.M. Smith, M.C. Mancini, S. Nie, Second window for *in vivo* imaging, *Nat. Nanotechnol.* 4 (2009) 710–711.
- [96] Y. Liu, J. Yang, B. Liu, W. Cao, J. Zhang, Y. Yang, L. Ma, J.M. de la Fuente, J. Song, J. Ni, C. Zhang, D. Cui, Human iPSC cells loaded with MnO₂-based nanoprobles for photodynamic and simultaneous enhanced immunotherapy against cancer, *Nano-Micro Lett.* 12 (2020) 127.
- [97] M.C. Ortega-Liebana, M.M. Encabo-Berzosa, A. Casanova, M.D. Pereboom, J. O. Alda, J.L. Hueso, J. Santamaría, Upconverting carbon nanodots from Ethylenediaminetetraacetic Acid (EDTA) as near-infrared activated phototheranostic agents, *Chem. A Eur. J.* 25 (2019) 5539–5546.
- [98] H. Zhu, J. Li, X. Qi, P. Chen, K. Pu, Oxygenic hybrid semiconducting nanoparticles for enhanced photodynamic therapy, *Nano Lett.* 18 (2018) 586–594.
- [99] J.F.C. Loo, Y.H. Chien, F. Yin, S.K. Kong, H.P. Ho, K.T. Yong, Upconversion and downconversion nanoparticles for biophotonics and nanomedicine, *Coord. Chem. Rev.* 400 (2019), 213042.
- [100] L. Colombeau, S. Acherar, F. Baros, P. Arnoux, A.M. Gazzali, K. Zaghdoudi, M. Toussaint, R. Vanderesse, C. Frochet, Inorganic nanoparticles for photodynamic therapy, *Top. Curr. Chem.* 370 (2016) 113–134.
- [101] L. Yang, C. Ren, M. Xu, Y. Song, Q. Lu, Y. Wang, Y. Zhu, X. Wang, N. Li, Rod-shape inorganic biomimetic mutual-reinforcing MnO₂-Au nanozymes for catalysis-enhanced hypoxic tumor therapy, *Nano Res.* 13 (2020) 2246–2258.
- [102] X.D. Zhang, D. Wu, X. Shen, J. Chen, Y.M. Sun, P.X. Liu, X.J. Liang, Size-dependent radiosensitization of PEG-coated gold nanoparticles for cancer radiation therapy, *Biomaterials* 33 (2012) 6408–6419.
- [103] Z. Wang, Y. Zhang, E. Ju, Z. Liu, F. Cao, Z. Chen, J. Ren, X. Qu, Biomimetic nanoflowers by self-assembly of nanozymes to induce intracellular oxidative damage against hypoxic tumors, *Nat. Commun.* 9 (2018) 3334.
- [104] Y. Ishida, Y. Agata, K. Shibahara, T. Honjo, Induced expression of PD-1, a novel member of the immunoglobulin gene superfamily, upon programmed cell death, *EMBO J.* 11 (1992) 3887–3895.
- [105] G.J. Freeman, A.J. Long, Y. Iwai, K. Bourque, T. Chernova, H. Nishimura, L.J. Fitz, N. Malenkovich, T. Okazaki, M.C. Byrne, H.F. Horton, L. Fouser, L. Carter, V. Ling, M.R. Bowman, B.M. Carreno, M. Collins, C.R. Wood, T. Honjo, Engagement of the Pd-1 immunoinhibitory receptor by a novel B7 family member leads to negative regulation of lymphocyte activation, *J. Exp. Med.* 192 (2000) 1027–1034.
- [106] M.Z. Noman, G. Desantis, B. Janji, M. Hasmim, S. Karray, P. Dessen, V. Bronte, S. Chouaib, PD-L1 is a novel direct target of HIF-1 α , and its blockade under

- hypoxia enhanced MDSC-mediated T cell activation, *J. Exp. Med.* 211 (2014) 781–790.
- [107] A. Facciabene, X. Peng, I.S. Hagemann, K. Balint, A. Barchetti, L.P. Wang, P. A. Gimotty, C.B. Gilks, P. Lal, L. Zhang, G. Coukos, Tumour hypoxia promotes tolerance and angiogenesis via CCL28 and Treg cells, *Nature* 475 (2011) 226–230.
- [108] J.W. Pollard, Tumour-educated macrophages promote tumour progression and metastasis, *Nat. Rev. Cancer* 4 (2004) 71–78.
- [109] Q. Sun, F. He, C. Sun, X. Wang, C. Li, J. Xu, D. Yang, H. Bi, S. Gai, P. Yang, Honeycomb-satellite structured pH/H₂O₂-responsive degradable nanoplatform for efficient photodynamic therapy and multimodal imaging, *ACS Appl. Mater. Interfaces* 10 (2018) 33901–33912.
- [110] L. Tian, Q. Chen, X. Yi, J. Chen, C. Liang, Y. Chao, K. Yang, Z. Liu, Albumin-templated manganese dioxide nanoparticles for enhanced radioisotope therapy, *Small* 13 (2017), 1700640.
- [111] R. Song, M. Zhang, Y. Liu, Z. Cui, H. Zhang, Z. Tang, X. Chen, H. Wu, Z. Yao, M. He, W. Bu, A multifunctional nanotheranostic for the intelligent MRI diagnosis and synergistic treatment of hypoxic tumor, *Biomaterials* 175 (2018) 123–133.
- [112] Q. Wu, G. Chen, K. Gong, J. Wang, X. Ge, X. Liu, S. Guo, F. Wang, MnO₂-laden black phosphorus for MRI-guided synergistic PDT, PTT, and chemotherapy, *Matter* 1 (2019) 496–512.
- [113] Y. Su, X. Zhang, L. Lei, B. Liu, S. Wu, J. Shen, Tumor microenvironment-activatable cyclic cascade reaction to reinforce multimodal combination therapy by destroying the extracellular matrix, *ACS Appl. Mater. Interfaces* 13 (2021) 12960–12971.
- [114] J.H. Yan, W. Meng, H. Shan, X.P. Zhang, L.M. Zou, L.L. Wang, J.S. Shi, X.Y. Kong, Melanin nanoparticles combined with CaO₂ nanoparticles for image-guided tumor microenvironment-responsive multimodal therapy, *ACS Appl. Nano Mater.* 4 (2021) 1351–1363.
- [115] J. Bonet-Aleta, M. Encinas-Gimenez, E. Urriolabeitia, P. Martin-Duque, J. L. Hueso, J. Santamaria, Unveiling the interplay between homogeneous and heterogeneous catalytic mechanisms in copper–iron nanoparticles working under chemically relevant tumour conditions, *Chem. Sci.* 13 (2022) 8307–8320.
- [116] N. Traverso, R. Ricciarelli, M. Nitti, B. Marengo, A.L. Furfaro, M.A. Pronzato, U. M. Marinari, C. Domenicotti, Role of glutathione in cancer progression and chemoresistance, *Oxid. Med. Cell Longev.* 2013 (2013), 972913.
- [117] E.A. Bump, J.M. Brown, Role of glutathione in the radiation response of mammalian cells *in vitro* and *in vivo*, *Pharmacol. Ther.* 47 (1990) 117–136.
- [118] M. Cox, D. Nelson, *Lehninger principles of biochemistry*, 2000.
- [119] C. Liang, X. Zhang, M. Yang, X. Dong, Recent progress in ferroptosis inducers for cancer therapy, *Adv. Mater.* 31 (2019), 1904197.
- [120] H. Fan, Z. Zhao, G. Yan, X. Zhang, C. Yang, H. Meng, Z. Chen, H. Liu, W. Tan, A smart DNzyme–MnO₂ nanosystem for efficient gene silencing, *Angew. Chem. Int. Ed.* 54 (2015) 4801–4805.
- [121] H. Fan, G. Yan, Z. Zhao, X. Han, W. Zhang, H. Liu, X. Fu, T. Fu, X.B. Zhang, W. Tan, A smart photosensitizer–manganese dioxide nanosystem for enhanced photodynamic therapy by reducing glutathione levels in cancer cells, *Angew. Chem. Int. Ed.* 55 (2016) 5477–5482.
- [122] S. Wang, F. Li, R. Qiao, X. Hu, H. Liao, L. Chen, J. Wu, H. Wu, M. Zhao, J. Liu, R. Chen, X. Ma, D. Kim, J. Sun, T.P. Davis, C. Chen, J. Tian, T. Hyeon, D. Ling, Arginine-rich manganese silicate nanobubbles as a ferroptosis-inducing agent for tumor-targeted theranostics, *ACS Nano* 12 (2018) 12380–12392.
- [123] J. Xu, W. Han, P. Yang, T. Jia, S. Dong, H. Bi, A. Gulzar, D. Yang, S. Gai, F. He, J. Lin, C. Li, Tumor microenvironment-responsive mesoporous MnO₂-coated upconversion nanoplatform for self-enhanced tumor theranostics, *Adv. Funct. Mater.* 28 (2018), 1803804.
- [124] H. Min, J. Wang, Y. Qi, Y. Zhang, X. Han, Y. Xu, J. Xu, Y. Li, L. Chen, K. Cheng, G. Liu, N. Yang, Y. Li, G. Nie, Biomimetic metal–organic framework nanoparticles for cooperative combination of antiangiogenesis and photodynamic therapy for enhanced efficacy, *Adv. Mater.* 31 (2019), 1808200.
- [125] X. Zhang, F.G. Wu, P. Liu, N. Gu, Z. Chen, Enhanced fluorescence of gold nanoclusters composed of HAuCl₄ and histidine by glutathione: glutathione detection and selective cancer cell imaging, *Small* 10 (2014) 5170–5177.
- [126] J. Ruan, H. Liu, B. Chen, F. Wang, W. Wang, Z. Zha, H. Qian, Z. Miao, J. Sun, T. Tian, Y. He, H. Wang, Interfacially engineered ZnMn_{1-x}S@Polydopamine hollow nanospheres for glutathione depleting photothermally enhanced chemodynamic therapy, *ACS Nano* 15 (2021) 11428–11440.
- [127] C. Liu, D. Wang, S. Zhang, Y. Cheng, F. Yang, Y. Xing, T. Xu, H. Dong, X. Zhang, Biodegradable biomimetic copper/manganese silicate nanospheres for chemodynamic/photodynamic synergistic therapy with simultaneous glutathione depletion and hypoxia relief, *ACS Nano* 13 (2019) 4267–4277.
- [128] L.H. Fu, Y.R. Hu, C. Qi, T. He, S. Jiang, C. Jiang, J. He, J. Qu, J. Lin, P. Huang, Biodegradable manganese-doped calcium phosphate nanotheranostics for traceable cascade reaction-enhanced anti-tumor therapy, *ACS Nano* 13 (2019) 13985–13994.
- [129] B. Ding, P. Zheng, F. Jiang, Y. Zhao, M. Wang, M. Chang, P.a. Ma, J. Lin, MnOx nanospikes as nanoadjuvants and immunogenic cell death drugs with enhanced antitumor immunity and antimetastatic effect, *Angew. Chem. Int. Ed.* 59 (2020) 16381–16384.
- [130] X. Lin, R. Zhu, Z. Hong, X. Zhang, S. Chen, J. Song, H. Yang, GSH-responsive radiosensitizers with deep penetration ability for multimodal imaging-guided synergistic radio-chemodynamic cancer therapy, *Adv. Funct. Mater.* 31 (2021), 2101278.
- [131] J. Ou, H. Tian, J. Wu, J. Gao, J. Jiang, K. Liu, S. Wang, F. Wang, F. Tong, Y. Ye, L. Liu, B. Chen, X. Ma, X. Chen, F. Peng, Y. Tu, MnO₂-based nanomotors with active fenton-like Mn²⁺ delivery for enhanced chemodynamic therapy, *ACS Appl. Mater. Interfaces* 13 (2021) 38050–38060.
- [132] X. Jin, M. Park, S.J. Shin, Y. Jo, M.G. Kim, H. Kim, Y.M. Kang, S.J. Hwang, Synergistic control of structural disorder and surface bonding nature to optimize the functionality of manganese oxide as an electrocatalyst and a cathode for Li–O₂ batteries, *Small* 16 (2020), 1903265.
- [133] J. Hedberg, E. Blomberg, I. Odnevall Wallinder, In the search for nanospecific effects of dissolution of metallic nanoparticles at freshwater-like conditions: a critical review, *Environ. Sci. Technol.* 53 (2019) 4030–4044.
- [134] S.E. Moriarty-Craige, D.P. Jones, Extracellular thiols and thiol/disulfide redox in metabolism, *Annu. Rev. Nutr.* 24 (2004) 481–509.
- [135] O. Lyublinskaya, F. Antunes, Measuring intracellular concentration of hydrogen peroxide with the use of genetically encoded H₂O₂ biosensor HyPer, *Redox. Biol.* 24 (2019), 101200.
- [136] L. Au, B. Lim, P. Colletti, Y.S. Jun, Y. Xia, Synthesis of gold microplates using bovine serum albumin as a reductant and a stabilizer, *Chem. Asian J.* 5 (2010) 123–129.
- [137] Y.N. Kozlov, K.G. Tikhonov, O.M. Zastrzhnaya, V.V. Klimov, pH dependence of the composition and stability of Mn(III)-bicarbonate complexes and its implication for redox interaction of Mn(II) with photosystemII, *J. Photochem. Photobiol. B, Biol.* 101 (2010) 362–366.
- [138] J.J. Pignatello, E. Oliveros, A. MacKay, Advanced oxidation processes for organic contaminant destruction based on the fenton reaction and related chemistry, *Crit. Rev. Environ. Sci. Technol.* 36 (2006) 1–84.
- [139] J. He, X. Yang, B. Men, D. Wang, Interfacial mechanisms of heterogeneous Fenton reactions catalyzed by iron-based materials: a review, *J. Environ. Sci.* 39 (2016) 97–109 (China).
- [140] Z.H. Meng, S.H. Wu, S.W. Sun, Z. Xu, X.C. Zhang, X.M. Wang, Y. Liu, H.T. Ren, S. Y. Jia, H. Bai, X. Han, Formation and oxidation reactivity of MnO₂–(HCO₃)_n in the MnII(HCO₃)_n–H₂O₂ system, *Inorg. Chem.* 59 (2020) 3171–3180.
- [141] E. Ember, H.A. Gazzaz, S. Rothbart, R. Puchta, R. van Eldik, MnII—A fascinating oxidation catalyst: mechanistic insight into the catalyzed oxidative degradation of organic dyes by H₂O₂, *Appl. Catal. B* 95 (2010) 179–191.
- [142] W. Zhu, N.G.J. Richards, Biological functions controlled by manganese redox changes in mononuclear Mn-dependent enzymes, in: S.J. Lippard, J.M. Berg (Eds.), *Bioinorganic Chemistry*, Portland Press Ltd, London, 2017, pp. 259–270.
- [143] P. Chen, J. Bornhorst, M. Aschner, Manganese metabolism in humans, *Front. Biosci. Landmark* 23 (2018) 1655–1679.
- [144] J. Bornhorst, S. Meyer, T. Weber, C. Böker, T. Marschall, A. Mangerich, S. Beneke, A. Bürkelt, T. Schwerdtle, Molecular mechanisms of Mn induced neurotoxicity: RONS generation, genotoxicity, and DNA-damage response, *Mol. Nutr. Food Res.* 57 (2013) 1255–1269.
- [145] Z. Mate, E. Horvath, G. Kozma, T. Simon, Z. Konya, E. Paulik, A. Papp, A. Szabo, Size-dependent toxicity differences of intratracheally instilled manganese oxide nanoparticles: conclusions of a subacute animal experiment, *Biol. Trace Elem. Res.* 171 (2016) 156–166.
- [146] A.M. Schrand, M.F. Rahman, S.M. Hussain, J.J. Schlager, D.A. Smith, S.F. Ali, Metal-based nanoparticles and their toxicity assessment, *Wiley Interdiscip. Rev. Nanomed. Nanobiotechnol.* 2 (2010) 544–568.
- [147] V.C. Culotta, M. Yang, M.D. Hall, Manganese transport and trafficking: lessons learned from *Saccharomyces cerevisiae*, *Eukaryot. Cell.* 4 (2005) 1159–1165.
- [148] R.O. Watson, S.L. Bell, D.A. MacDuff, J.M. Kimmey, E.J. Diner, J. Olivas, R. E. Vance, C.L. Stallings, H.W. Virgin, J.S. Cox, The cytosolic sensor cGAS detects mycobacterium tuberculosis DNA to induce type I interferons and activate autophagy, *Cell Host Microbe* 17 (2015) 811–819.
- [149] C. Wang, Y. Guan, M. Lv, R. Zhang, Z. Guo, X. Wei, X. Du, J. Yang, T. Li, Y. Wang, X. Su, X. Huang, Z. Jiang, Manganese increases the sensitivity of the cGAS–STING pathway for double-stranded DNA and is required for the host defense against DNA viruses, *Immunity* 48 (2018) 675–687, e677.
- [150] M. Yu, J. Zheng, Clearance pathways and tumor targeting of imaging nanoparticles, *ACS Nano* 9 (2015) 6655–6674.
- [151] J. Tan, X. Duan, F. Zhang, X. Ban, J. Mao, M. Cao, S. Han, X. Shuai, J. Shen, Theranostic nanomedicine for synergistic chemodynamic therapy and chemotherapy of orthotopic glioma, *Adv. Sci.* 7 (2020), 2003036.
- [152] J. Xu, R. Shi, G. Chen, S. Dong, P. Yang, Z. Zhang, N. Niu, S. Gai, F. He, Y. Fu, J. Lin, All-in-one theranostic nanomedicine with ultrabright second near-infrared emission for tumor-modulated bioimaging and chemodynamic/photodynamic therapy, *ACS Nano* 14 (2020) 9613–9625.
- [153] Q. Zhang, D. Dehaini, Y. Zhang, J. Zhou, X. Chen, L. Zhang, R.H. Fang, W. Gao, L. Zhang, Neutrophil membrane-coated nanoparticles inhibit synovial inflammation and alleviate joint damage in inflammatory arthritis, *Nat. Nanotechnol.* 13 (2018) 1182–1190.
- [154] Z. Chen, P. Zhao, Z. Luo, M. Zheng, H. Tian, P. Gong, G. Gao, H. Pan, L. Liu, A. Ma, H. Cui, Y. Ma, L. Cai, Cancer cell membrane–biomimetic nanoparticles for homologous-targeting dual-modal imaging and photothermal therapy, *ACS Nano* 10 (2016) 10049–10057.
- [155] X. Shen, W. Liu, X. Gao, Z. Lu, X. Wu, X. Gao, Mechanisms of oxidase and superoxide dismutation-like activities of gold, silver, platinum, and palladium, and their alloys: a general way to the activation of molecular oxygen, *J. Am. Chem. Soc.* 137 (2015) 15882–15891.
- [156] M.C. Ortega-Liebana, J. Bonet-Aleta, J.L. Hueso, J. Santamaria, Gold-based nanoparticles on amino-functionalized mesoporous silica supports as nanozymes for glucose oxidation, *Catalysts* 10 (2020).
- [157] M.V. Libertini, J.W. Locasale, The warburg effect: how does it benefit cancer cells? *Trends Biochem. Sci.* 41 (2016) 211–218.

- [158] R.J. DeBerardinis, J.J. Lum, G. Hatzivassiliou, C.B. Thompson, The biology of cancer: metabolic reprogramming fuels cell growth and proliferation, *Cell Metab.* 7 (2008) 11–20.
- [159] J.S. Burns, G. Manda, Metabolic pathways of the warburg effect in health and disease: perspectives of choice, chain or chance, *Int. J. Mol. Sci.* 18 (2017) 28.
- [160] A. Ciucu, C. Pătroescu, Fast spectrometric method of determining the activity of glucose oxidase, *Anal. Lett.* 17 (1984) 1417–1427.
- [161] Y. Meng, K. Zhao, Z. Zhang, P. Gao, J. Yuan, T. Cai, Q. Tong, G. Huang, D. He, Effects of crystal structure on the activity of MnO₂ nanorods oxidase mimics, *Nano Res.* 13 (2020) 709–718.
- [162] X. Zhang, Y. Junhui, Y. Jing, C. Ting, X. Bei, L. Zhe, Z. Kunfeng, Y. Ling, H. Dannong, Excellent low-temperature catalytic performance of nanosheet Co-Mn oxides for total benzene oxidation, *Appl. Catal. A* 566 (2018) 104–112.
- [163] E. Hayashi, Y. Yamaguchi, K. Kamata, N. Tsunoda, Y. Kumagai, F. Oba, M. Hara, Effect of MnO₂ crystal structure on aerobic oxidation of 5-hydroxymethylfurfural to 2,5-furandicarboxylic acid, *J. Am. Chem. Soc.* 141 (2019) 890–900.
- [164] Q. Li, J. Ren, Q. Chen, W. Liu, Z. Xu, Y. Cao, Y. Kang, P. Xue, A HMCuS@MnO₂ nanocomplex responsive to multiple tumor environmental clues for photoacoustic/fluorescence/magnetic resonance trimodal imaging-guided and enhanced photothermal/photodynamic therapy, *Nanoscale* 12 (2020) 12508–12521.
- [165] S. Mukherjee, C.R. Patra, Therapeutic application of anti-angiogenic nanomaterials in cancers, *Nanoscale* 8 (2016) 12444–12470.